

Semi-Annual Report
January 1968

ADHESION BETWEEN ATOMICALLY PURE METALLIC SURFACES

PART IV

GPO PRICE \$ _____

CFSTI PRICE(S) \$ _____

Hard copy (HC) 300

Microfiche (MF) 65

by

D. V. Keller, Jr.

ff 653 July 65

Associate Professor of Metallurgy

Department of Chemical Engineering and Metallurgy

with

T. McNicholas Research Assistant

FACILITY FORM 602	N68-17654	
	(ACCESSION NUMBER)	(THRU)
	<u>76</u> (PAGES)	<u>1</u> (CODE)
	<u>CP#93248</u> (NASA CR OR TMX OR AD NUMBER)	<u>17</u> (CATEGORY)

Prepared for

National Aeronautics and Space Administration

Office of Grants and Research Contracts, Code SC

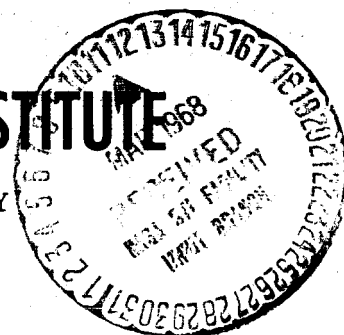
Washington, D.C.

Grant No. NSG-483-1



SYRACUSE UNIVERSITY RESEARCH INSTITUTE

DEPARTMENT OF CHEMICAL ENGINEERING AND METALLURGY
MET-1100-6801-SA



♦ Semi-Annual Report
January 1968

ADHESION BETWEEN ATOMICALLY PURE METALLIC SURFACES

PART IV

by

D. V. Keller, Jr.

Associate Professor of Metallurgy

Department of Chemical Engineering and Metallurgy

with

T. McNicholas - Research Assistant

Prepared for

National Aeronautics and Space Administration

Office of Grants and Research Contracts, Code SC

Washington, D.C.

Grant No. NsG-483-1

This report was produced under a sponsored contract. The conclusions and recommendations expressed are those of the Author and are not necessarily endorsed by the Sponsor. Reproduction of this report, or any portion thereof, must bear reference to the original source and Sponsor.

SYRACUSE UNIVERSITY RESEARCH INSTITUTE

Department of Chemical Engineering and Metallurgy

MET-1100-6801-SA

PREFACE

The January 1968 Semi-Annual Report consists of a Master's Degree Thesis by T. McNicholas, which reviews in depth the analysis of metallic adhesion data obtained from iron-65 parts per million carbon couples. Due to the breadth of the information contained in this thesis, including a discussion of the automatic testing technique, continuous recording of contact resistance versus load data, theoretical interpretation of these curves and the initial presentation of interfacial creep data with a tentative analysis, it was felt that further exploitation of the data contained therein ought to remain until the confirming ultra pure iron studies are complete.

The ultra pure iron (8 ppm carbon) investigations which will be initiated in the near future will serve to test the proposed analytical techniques for contact area change with load and with time at constant load as described in the thesis. In the event that analytical consistency between the two material systems is found for these preliminary explorations, a more quantitative study of each of the various aspects will be undertaken. For example, the results of the Fe-65ppm carbon study indicate that there exists three significant stages in the deformation of asperities as two bulk surfaces are brought together. The first is involved in bringing the number of point contacts to an equilibrium state such that this number is constant; and therefore the recorded information reflects the state of deformation at the interface. This should be true for all systems irrespective of the chemistry of the system. The second stage, or the steady state deformation of the asperities at a constant number of contact points, is due to the bulk deformation of the material in the asperities which may, or may not be a function of the chemistry

of the system. Since the following studies only intend to vary the carbon content of the sytem, one might suspect that this stage ought to be similar whether or not carbon is present particularly when the carbon can only be present in a few atomic layers (Fe-65ppm C). The third stage, creep, may also be altered in the ultra pure iron case since creep is expected to involve the surficial layers of the asperities in expanding the real contact area per unit time.

Probably the ultimate test of the proposed analysis, however, will be the correspondence of the observed contact resistance curve with the theoretical curve utilizing the bulk resistivity of ultra pure iron rather than that used for this investigation, cf. text.

INVESTIGATION OF THE ADHESION BETWEEN
ULTRA CLEAN IRON-65ppm CARBON COUPLES
UTILIZING CONTACT RESISTANCE TECHNIQUES

BY

THOMAS MARTIN MCNICHOLAS

Polytechnic Institute of Brooklyn
Brooklyn, New York
B.S. (Metallurgy), 1961

THESIS

Submitted in partial fulfillment of the requirements
for the degree of Master of Science in Metallurgy in
the Graduate School of Syracuse University.

Approved _____

Date _____

ABSTRACT

The metallic adhesion characteristics of an iron-65ppm carbon couple were investigated using the technique of Johnson and Keller which was refined by a continuous recording of the contact resistance and load data on an x-y recorder. Contact resistance results approximate closely theoretical curves which consider surface asperity phenomena. Bulk metallic adhesion was not characteristic of the system; to explain this, a model of carbon contamination of the surface by bulk diffusion is suggested. Creep processes found in the plastic range of the asperities are outlined and found to be in agreement with bulk plastic values.

ACKNOWLEDGEMENTS

The author wishes to express his sincere gratitude to his Thesis Advisor, Dr. Douglas V. Keller, Jr., for his guidance and help during the course of this investigation. He gratefully acknowledges the Personnel of the Metallurgical Research Laboratories of Syracuse University for their assistance, in particular Miss Martha Coleman who typed this paper and was a model of patience. A special thanks is due to his family and dear friends.

The author is also indebted to the National Aeronautics and Space Administration for financial support provided under Grant No. NSG-483-1.

CONTENTS

	PAGE
ACKNOWLEDGEMENT.	ii
I. INTRODUCTION	1
Metallic Adhesion.	1
Metallic Adhesion Theory	4
Contamination in Metallic Adhesion	8
Other Variables.	12
Real Surfaces.	13
Contact Resistance Theory.	16
II. EXPERIMENTAL	20
Material	20
Apparatus.	20
Procedure.	31
III. RESULTS AND DISCUSSION	34
Contact Resistance	34
Adhesion	46
Creep.	55
IV. CONCLUSIONS AND RECOMMENDATIONS.	61
V. BIBLIOGRAPHY	63
BIOGRAPHICAL DATA.	67

LIST OF FIGURES

FIGURE		PAGE
1	VARIATION IN THE PLOWING AND ADHESION COMPONENTS OF THE COEFFICIENT OF FRICTION.	5
2	BEHAVIOR OF A CONTACT UNDER HIGH PRESSURE.	15
3	LONGITUDINAL MICROSTRUCTURE OF 99.993% IRON-65ppm CARBON SPECIMENS.	21
4	VACUUM SYSTEM.	22
5	ADHESION CELL.	24
6	RECORDING CIRCUIT.	28
7	ADHESION TEST APPARATUS.	33
8	INFORMATION FROM CONTINUOUS ADHESION PLOT.	35
9	TYPICAL "x-y" PLOT FOR IRON-65ppm CARBON ADHESION CYCLE. . . .	37
10	TYPICAL ADHESION CYCLES ON THE SAME CONTACT POINT.	38
11	EXPANDED SCALE OF FIGURE 10.	39
12	THEORETICAL CURVES UNDER VARIOUS CONDITIONS OF MULTIPOINT CONTACT.	42
13	COMPARISON OF THEORETICAL AND OBSERVED CURVES.	44
14	LOADING CONDITIONS IN THE CONTACT INTERFACE.	54
15	CONTACT RESISTANCE CREEP CURVES.	58

I. INTRODUCTION

A detailed description of adhesion phenomena includes a precise pre-contact characterization of the two free surfaces concerned, the morphology and energetics of the contacting process, and the mechanism of junction failure when the system is placed in tension (1,2). The purpose of this experimental investigation is a detailed examination of the various stages of the adhesion process, by utilizing the variation of the contact resistance between two ultra pure iron samples contaminated with 65 parts per million (ppm) carbon. The introduction of this paper has been subdivided to correspond to those areas of particular interest to metallic adhesion and to the means of experimental observation.

Metallic Adhesion

Understanding the phenomena accompanying the contact of two solid metallic surfaces is of immense scientific and engineering interest (3). Directly concerned are the economically important processes of friction, lubrication and wear of metallic components, as well as surface interactions involved in machining, metal forming and joining, and powder metallurgical techniques. With technology continuing to extend the limits of our knowledge, these processes have been subjected to greater and greater demands as new materials become available and operating conditions are expanded to include more complex designs and extreme environments (4). The underlying principles of each topic, however, appear to have been developed largely as an independent entity, such that the current theories of a particular discipline reflect only the relevant details of that

particular process (5), as a consequence, many of the processes appearing to be divergent are actually related to the one basic mechanism, i.e. surface contact phenomena. The phenomena of adhesion, which is defined as the nature of the attractive force between two surfaces (1), treats this very problem from a fundamental aspect. Therefore, the principles of the mechanism of metallic adhesion can and are used, in part, to account for some of the surface interaction processes which are involved in friction and wear, and numerous metallic bonding, removal and forming operations.

One example of such an application within the last 20 years is the interdisciplinary approach (6,7) to friction which has been very fruitful in elucidating the relative significance of the varied aspects of this process.

Because of the limits of scientific technology, classical workers derived a theory of friction based on the macro properties of the system. Friction was considered to be the force required to lift asperities, or surface micro-irregularities, over one another. Amontons (1699) compared the lifting of asperities to the raising of a load on an incline plane. Coulomb (1785) refined these geometrical and mechanical concepts further by considering the entanglement of asperities on each surface. Three empirical laws were resolved from the classical theories (8):

1. The friction force is directly proportional to the load.
2. The frictional force for a constant load is independent of the apparent area of contact.
3. The frictional force depends upon the nature of the materials in contact.

However, these relations did not explain the observed losses of energy during sliding. When the laws of plastic and elastic deformation of solids evolved and were applied to the manner in which asperities deformed, it became clear that the actual contact of surfaces was indeed controlled by the same mechanisms. Tabor (2) recognized that in addition to the irreversible deformation of one set of asperities by another, a second primary dissipative process arose from the breaking of adhesion at the points of cold-welded contact. The attractive force between atoms in the contact interface was thought to exist just as do the attractive and repulsive fields surrounding an atom in a solid which supports a normal load (9,10).

The generally accepted concept of the friction force (F) between unlubricated surfaces (7) can be expressed as the sum of two forces resisting tangential motion; e.g. the force required to shear adhesion junctions (F_A) and the force to plow asperities through each other (F_D).

$$F = F_{\text{Adhesion}} + F_{\text{Deformation}} \quad \text{EQUATION 1}$$

If both the adhesion and "plowing" term are considered to act independently, the deformation term can be expressed as P , and the adhesive term as a function of the real contact area A and the average force (s) required to shear the material bridging the gap between surfaces.

$$F = As + P \quad \text{EQUATION 2}$$

Because of the importance and consistency of this relation, the main variables and their effects on the total friction force have been scrutinized in detail by numerous workers (11). Most of the recent research effort has been exerted

towards a better understanding of the real contact area (12), the shear strength of the adhesive interface and the adhesive force between surfaces (11), interaction of A and s with each other and with the deformation term (13), and the deformation term itself (14).

Bowden, Tabor (7) and Steijn (15) have shown the adhesion term to be the preponderant factor unless masked by gross surface contamination and/or extremely high loads. Using a mechanical treatment, Goddard and Wilman (14) derived several relations involving the deformation term, which have been characterized and expanded by the experimental work of Steijn (15) and others (16,17). This aspect is exemplified by the plot in Figure 1, acquired from data on the movement of a diamond stylus of 76μ radius over the surface of a polycrystalline copper plate (15).

Such investigations illustrate the significance of the adhesion term, and consequently the adhesion process. Since most real friction applications involve much lighter loads than those illustrated, a higher dependence on the adhesion term is expected.

Metallic Adhesion Theory

Keller (18) recently classified the techniques for the analysis of metallic adhesion data into four sub-groups: interfacial (surface tension), solution, electronic (dispersion and electrostatic) and fracture. Each analytical technique is based on a particular model of the interface system; for example, the first considers the interrelationship of the free surface energies relative to the resulting interface energy. Although this scheme is widely used in liquid-solid adhesion analysis, and in particular for

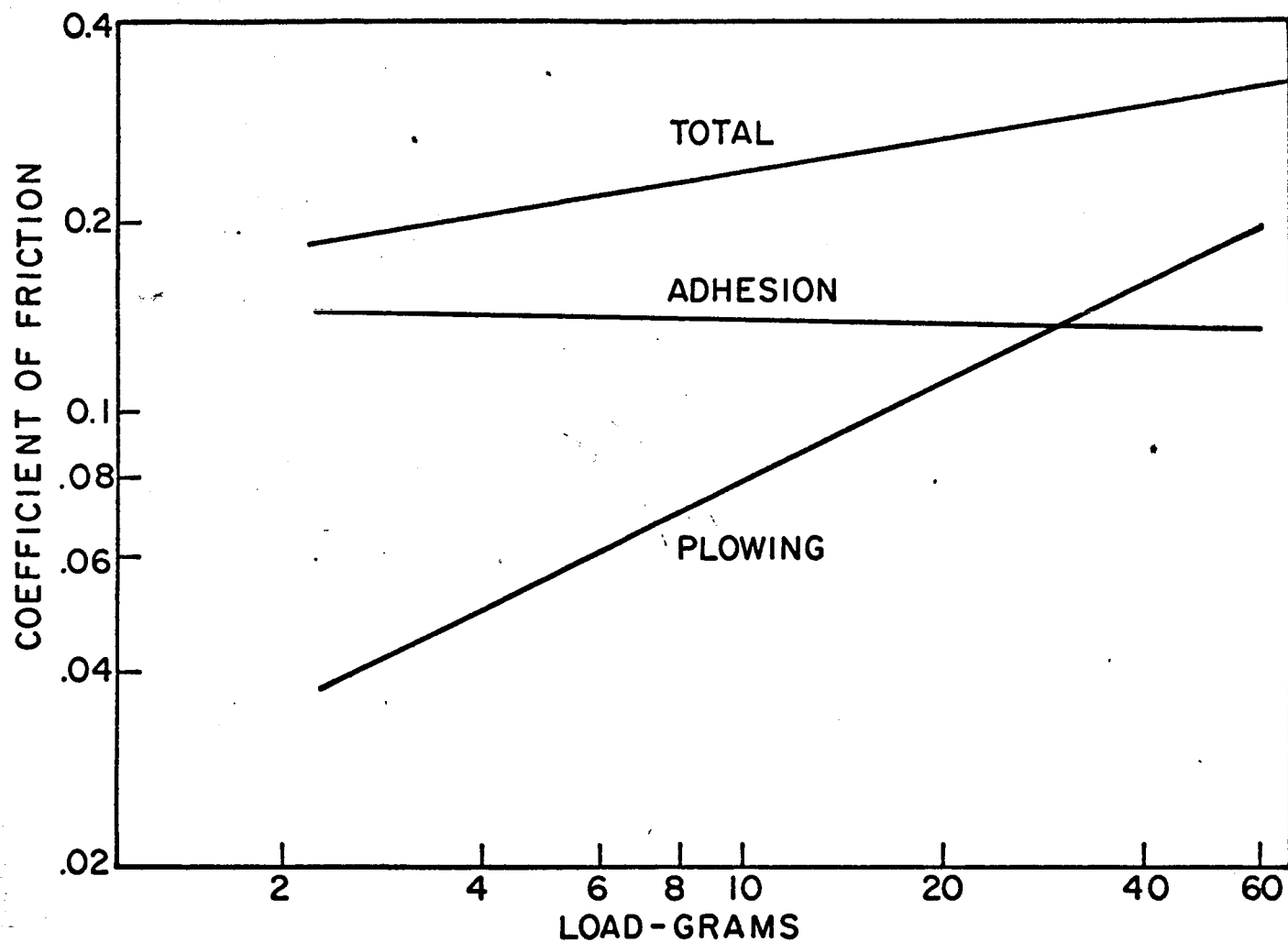


FIG. 1 VARIATION IN THE PLOWING AND ADHESION COMPONENTS OF THE COEFFICIENT OF FRICTION AND THE LOAD ON A 76μ RADIUS DIAMOND STYLUS MOVING ON POLYCRYSTALLINE COPPER (15)

organic systems, it has not found great success in metallic system analysis due to the lack of reliable interfacial energy data. The lack of precise data also exists in the cases of the solution and electronic models; which may be cited as the main reason why such approaches have not produced fruitful results for adhesion analysis in metallic systems.

Since the fracture approach is currently the most popular, let us outline the principal steps which are involved in a typical adhesion experiment (2,19,20). Using a mechanical test apparatus, normally with a controlled atmosphere and/or temperature, two metal surfaces are placed into contact under a known normal load for a known duration. Then the load necessary to cause junction fracture is measured in pure tension. Clearly, the crack formed in tension will propagate down the interface region only if this is the weakest path in the system. For example, a diffusion bonded interface system could be cited as one case in which the interface could be much stronger than either bulk metal phase, while a well lubricated interface would present an exceedingly weak interface. Since the intent of this investigation is to examine interfaces of pure iron at room temperature, without contaminants, the extreme limits just mentioned will not be involved.

The quantitative analytical approach to metallic adhesion requires the formation of a simple ideal model of the system, which in turn, should lend to the design and understanding of a critical experiment, and significant data. There are numerous proposals for such models (2,18,21), and all are probably acceptable within certain qualifying limits as established

by the inherent variables in the system. The complexity of the system, i.e. the interaction of two real metallic surfaces, seems however, to have inhibited the success of previous models in a complete quantitative analysis of metallic adhesion. A simple model was recently proposed (22) which incorporates many facets of the previous models and stresses the more important aspects of the process.

Consider two perfect metallic crystal surfaces devoid of surface imperfections and contaminants in an ultimate vacuum at 0°K. If the two crystals are brought into a forceless contact, such that exact atomic coincidence is achieved along the interface, the resulting body should be a perfect single crystal in which the interface region is indistinguishable from the matrix of the perfect crystal. Since chemisorption on free metallic surfaces is a non-activation energy process (23), and the process just described is basically the same as chemisorption, one would not expect the process to require a separate activation energy of interface formation. Haneman and Grant (24) have added credibility to the interface model in their recent cleavage studies of germanium, and investigations of silicon-silicon epitaxy by Jona (25) also attest to the model.

The tensile strength and fracture mechanism of the crystal joined by the steps just cited ought to be identical with that of any single crystal of the same material and purity, since the interface is indistinguishable from the bulk.

Most systems involve polycrystalline material and contact under a normal load, therefore, one must further consider the changes in tensile

properties of the single crystal model if it is subjected to small compressive loads and/or rotation of one of the crystals before contact is made. The former has little effect on the tensile fracture strength behavior unless the compressive yield point is grossly exceeded. Rotation of one of the single crystals prior to ideal contact would produce an interface which is quite similar to a grain boundary; in fact, if the system were permitted to come to thermal equilibrium, a grain boundary would result. The tensile strength of the grain boundary system should lie between that of the single crystal system and the polycrystalline system. Since a polycrystalline surface is an array of single crystal regions, the interface formed can be reduced to a summation of unaligned single crystal interactions across the boundary. Grain growth and the establishment of thermal equilibrium will reconstruct the interface such that it is indistinguishable from the matrix (26,27). In conclusion, we can assume that an interface between two atomically clean, polycrystalline metallic surfaces should produce a system in which the junction strength per unit area of real contact approaches that of the polycrystalline bulk metal.

Contamination in Metallic Adhesion

In evaluating a method to record the path followed during the critical experiment, we must consider the effects of real system variables on the model and the means of observation. The area of contact between real surfaces, and the effects of chemical contamination on the strength of the interface are the most influential factors in adhesion analysis (2,20,28). Electrical contact resistance methods (2,19,29) are considered the best

means of observing the deformation, adhesion and fracture process.

(See Experimental Section).

Contamination, i.e. the presence of low cleavage strength, foreign films in the interface region, has been shown to be the only major barrier to metallic adhesion approaching the strength of the bulk metal (19,20). The presence of a contaminant along the interface presents a plane of weakness along that interface which is followed by an advancing cleavage crack when the system is unloaded or placed in tension. Although such films have been used under the guise of "lubrication" for ages, precise knowledge of the extent to which a lubricant will inhibit the formation of a mechanically stable junction between metallic surfaces was not established until recent ultra high vacuum studies were completed. Johnson (20) illustrated that in some cases, e.g. Mo, Ti, a monolayer of adsorbed film could prevent full strength adhesion.

An event which may permit the contaminant layer to be bridged by intimate metal to metal contact will tend to strengthen the interfaces; therefore, the strength of a metallic adhesion junction may lie anywhere between the bulk strength of the metal and that of the contaminant layer, i.e. approximately zero. Normal contaminants (brittle oxides, certain chemisorbed gases, condensed organic vapors) usually provide a much weaker fracture plane than a metal-metal junction. The effects of pure physical constraints on establishing an area of real contact, such as surface roughness and non-metallic particles, will be discussed later.

Since the presence of only a few monolayers of a particular contaminant can reduce the junction strength to near zero between lightly loaded contacts (19,20), it is necessary to completely remove all possible contaminants prior to the study of adhesion in the nearly ideal model system. Thereafter, a selective study of contaminant films on the adhesion process is possible by adsorption or diffusion (30). The time required to contaminate a surface is very short, for example, if a monolayer is adsorbed from the gas phase (assuming a sticking probability of one), the clean surface life time is about one second at 10^{-6} Torr and a few hours at 10^{-10} Torr (31). Most workers (31,20) define a clean surface as that point when less than 10% of the free surface constitutes the contaminant phase. Achieving and verifying this condition is most difficult (32), cf. next section on contact resistance.

As previously inferred, a reasonable adhesion strength can also be obtained if sufficient energy is introduced into the interface to disperse the interfacial contaminants, thereby establishing pure metal-metal contact. Energy input processes such as heat, tangential motion, ultrasonics, etc. will cause bonding if sufficient energy is imparted to the interface during contact. Since precise energy input requirements and precise characterization of the dispersal rate of the contaminants to cause adhesion under atmospheric conditions are most difficult to establish, this aspect has only been pursued in a most qualitative manner. Sikorski (33,34) Milner (35) and others (36) have contributed significantly to adhesion studies under these conditions, utilizing the techniques of roll bonding, friction welding, and other commercial processes. The most significant advances in the

study of the mechanism of metallic adhesion have been achieved under conditions in which the contaminants have been rigorously controlled, i.e. ultra high vacuum.

Investigations of metallic adhesion under vacuum conditions of less than 10^{-9} Torr usually involve surfaces preparations by one of three techniques (37): fractured surface (26,38), argon ion bombardment and anneal (20,27) or by mechanical treatment such as wire brushing. The many inherent difficulties with wire brushing and fracture techniques have been thoroughly discussed elsewhere (37).

Argon ion bombardment of a surface is normally accomplished after the specimen and holder have been thoroughly outgassed by heating for many hours in ultra high vacuum. The cleaning process consists of the ionization of very pure argon in a field of less than 1KV. The surface to be cleaned is negatively charged with respect to the rest of the components. During the process, defects and dislocations are produced in the solid surface, and many inert gas atoms are embedded in the surface lattice. High temperature annealing treatment is necessary to permit the gas atoms to leave and to allow recrystallization to recover the highly distorted surface layers. Low energy electron diffraction (LEED) studies have verified this mechanism (39). The disadvantage of the technique lies in the post-cleaning anneal treatment which permits bulk impurities more than sufficient time to diffuse to the freshly cleaned surface and re-establish the contaminant layer. This has also been described in systems of carbon or oxygen in iron (40), titanium (41), and tungsten (42), to cite a few specific examples.

Other Variables

Since the mechanical properties of the load bearing contact area, the rates of vapor, bulk and surface diffusion, the interfacial chemistry of the system and the fracture behavior of a particular metal system are functions of temperature, it should not be surprising that temperature also has a profound effect on adhesion. For example, in a number of systems (27) contaminant layers interrupt junction strength at room temperature, but when these systems are subjected to higher temperatures, the contaminants are dispersed by dissolution and the full bulk metal adhesive strength can be achieved.

Immiscible dissimilar metal couples were thought to be poor candidates for making strong adhesive junctions as a result of early friction tests (43) and thermodynamic analysis (44,45). Recent observations (20,46) however, indicate that bulk immiscibility is not a criterion for adhesion, in accord with theoretical arguments (47-49), which delineate between chemical equilibrium of the surface phase and that of the bulk phase. Cahn and Hilliard (50) and others (49) have proposed an agreeable solid state interface model which considers an interface as a zone of concentration gradient on a regular solution model. Numerous LEED and molecular beam investigations appear to substantiate these observations.

Relationships involving the relation of adhesive strength to crystal structure (46,51-53), melting point (44) hardness (34,51) and various other materials properties have also been presented. Such would be expected, since the deformation properties of the interface region which controls the

extent of the contact area is also dependent on such properties. If however, the junction strength is measured by means of the true contact area (19,20), one finds that this strength is approximately equivalent to that of the weaker bulk metal, and little is gained through secondary material property relationships.

In tests to evaluate contaminated systems, some of the major system variables which must be strictly controlled to obtain reproducible results are: surface chemistry, geometry, roughness, material properties, pre-test vacuum treatments, specimen composition and metallurgy. All of these could individually cause considerable modifications in the contaminant layer dispersal mechanism and in turn the observed adhesive strength. A detailed discussion of each of these variables would be most extensive; and is consequently considered beyond the scope of this paper.

Real Surfaces

A real surface is considered to be extremely rough on a microscale (7, 54); therefore, when two such atomically clean surfaces are brought together, the size, shape and distribution of the high points (asperities) will determine the nature of the real contact area. The process of contact of two real bulk surfaces may be described in two stages; those mechanical deformation interactions which involve only the asperities, e.g. micro-processes, and those which involve the bulk, e.g. macro-processes. In the initial point to point contact the micro-deformation processes would involve elastic deformation of two or three asperities, however, since the peaks include only a very small region, normal observation would tend to

obscure these interactions. Thereafter, the plastic deformation of these asperities will occur until the load is supported on many asperities and by the bulk system either elastically or plastically depending on the load. The real area of contact and configuration of the load supporting interface is therefore determined by the modes of asperity deformation (54).

Since the yield pressure (P) for most metals is nearly constant, the contact area formed is proportional to the load on each of the individual asperities. Therefore, the total area (A) can be given by equation:

$$A = \frac{w_1}{P} + \frac{w_2}{P} + \frac{w_3}{P} + \dots = \frac{W}{P} \quad \text{EQUATION 3}$$

where W is the total applied load and w_1 is the load supported by one asperity.

Archard (55) has shown that even elastic Hertzian analysis can be made to approach a contact area proportional to load if one generalizes the model to cover each asperity with successive micro-asperities. The elastic model indicates that A is proportional to $W^{2/3}$, if the number of contacts is taken as constant, but if the average area of each contact remains constant, A is again proportional to W.

Greenwood and Williamson (12) extended the elastic model by studying asperities closely resembling those found on real surfaces (Gaussian distribution), and deformation exceeding the elastic limit. Again, the area of contact was found to be very nearly proportional to load in both plastic and elastic models.

Recently, Williamson (54) used a very precise profilimeter to examine an aluminum surface at various stages of deformation. He found (see Figure 2)

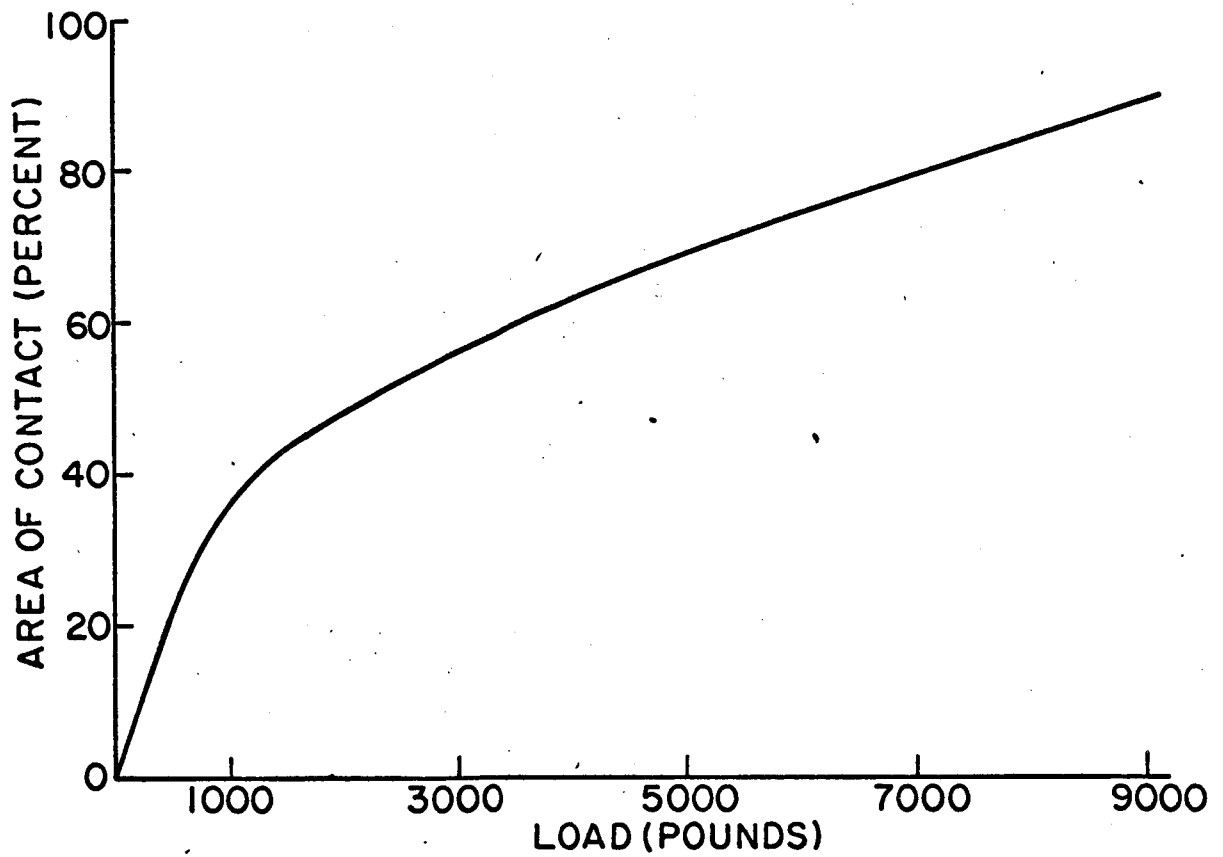
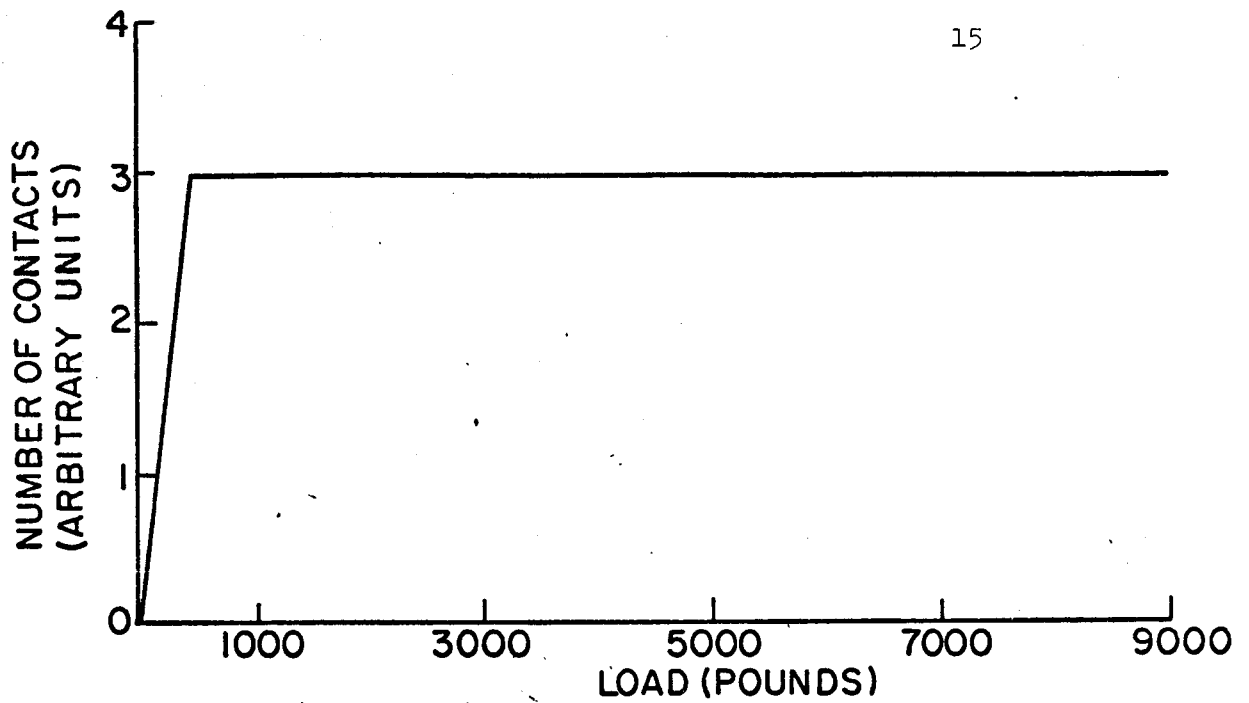


FIG.2 BEHAVIOR OF A CONTACT UNDER HIGH PRESSURE (54)
(SEE TEXT FOR DESCRIPTION)

that at light loads the real area of contact and the number of contacts are proportional to the load; but at higher loads the number of contact spots remains constant and their size increases with load.

By evaluating Hertzian contact area derivations (which assumes smooth surfaces and elastic interactions), Saunders (56) and others (19) found that at loads above the yield strength of the weaker metal specimen, Holm's contact resistance methods provided a more reliable technique to study the true contact area.

Contact Resistance Theory

Contact resistance measurements seem to offer the most promising tool for following the change in real contact area with load (18,28). The most influential variables (57-59) involved in the observed contact resistance between two crossed-rods are the effects of multipoint asperity contact, tunneling and contaminating films. The Gaussian distribution of the asperities and the relatively complete knowledge of resistance methods (29) have permitted a rather detailed analysis of the contact resistance versus load curve between two conductors to give the character of the deformation process.

Kisluk(59) has considered the effect of real surfaces on the observed contact resistance (R_o) and related this to the pure constriction resistance (R_c) by a factor of (R_f) caused by electron tunneling or contaminant film effects.

$$R_o = R_c \pm R_f$$

By using ultra-clean metallic surfaces and fixing the test geometry (crossed-wires), the effect of R_f can be assumed constant and negligible (29).

Holm (29) has shown that R_c in a system with a single point contact is

$$R_c = \frac{\rho}{2a} \quad \text{EQUATION 4}$$

where a is the contact radius of the true contact area and ρ is the conductivity of the pure bulk metal involved in the contact couple.

The variation of contact radius with load (W) was found by a relation developed by Holm (29) to depend on the deformation mechanism.

$$\begin{aligned} a &\propto W^{\frac{1}{3}} \quad (\text{for pure elastic deformation}) \\ a &\propto W^{\frac{1}{2}} \quad (\text{for pure plastic deformation}) \end{aligned} \quad \text{EQUATION 5}$$

Combining (4) and (5) we obtain the relationship between constriction resistance and the applied load.

$$\begin{aligned} R_c &\propto W^{-\frac{1}{3}} \quad (\text{elastic}) \\ R_c &\propto W^{-\frac{1}{2}} \quad (\text{plastic}) \end{aligned} \quad \text{EQUATION 6}$$

Greenwood (57) explored the effects of multiple micro-contacts on the constriction resistance and showed that

$$R_c \approx \frac{\rho}{2 \sum a_i} + \frac{\rho}{\pi n^2} \sum_{i \neq j} \sum \frac{1}{S_{ij}} \quad \text{EQUATION 7}$$

where ρ = resistivity of the bulk metal

a_i = radius of the i^{th} metal contact

n = number of contacts

S_{ij} = distance between the i^{th} and j^{th} contact

Since all real systems involve multicontact points, the Greenwood value for R_c must be related to a real area of contact (A). Greenwood also provided a relation between the area of contact (A_I) derived from Holm's single point equation 4 and the real area (A_N) of contact as derived from equation 7. The ratio may be roughly approximated by:

$$\frac{A_I}{A_N} = 1.4n^{\frac{1}{2}} \quad \text{EQUATION 8}$$

where the number of contacts (n) is assumed to be small (<50).

If we further assume that the A_N value represents the true area relationship and that the true area can be simply related to the yield strength of the bulk metal (Y) in simple plastic deformation (61), then a relationship between the observed contact resistance and load can be achieved:

$$\frac{A_I}{A_N} = 1.4n^{\frac{1}{2}} = \pi \frac{(\rho/2R_c)^2}{W/3Y} \quad \text{EQUATION 9}$$

rearranging

$$n^{1/4} R_c = 1.3\rho Y^{1/3} W^{-1/2} \quad \text{EQUATION 10}$$

For ultra pure iron, ρ is $9.7 \times 10^{-6} \Omega - \text{cm}$ (62) and Y is 2.5 kg/mm^2 (63)

Equation 10 becomes

$$n^{1/4} R_c = 6.3 \times 10^{-3} W^{-1/2} \quad \text{EQUATION 11}$$

Since the yield strength is expected to vary as a function of the continually changing work hardening of the asperities, equation 11 cannot be considered to be exact, but will serve as a reasonable approximation until a comparison with actual data (R_o) is made.

The relation of the number of contact points (n) to W will rapidly increase from one (first contact point) at an extremely light load, to some constant value as predicted by Williamson (54) (See Figure 2). When n becomes constant the value of R_c , or the change in contact area is directly related to the load. The slope of the $\log R_o$ versus $\log W$ plot is, therefore, directly related to the deformation mechanism of the asperities.

II. EXPERIMENTAL

Material

High purity iron (99.999%) 1.5 mm wire, was obtained from United Mineral and Chemical Corporation with a total impurity concentration of:

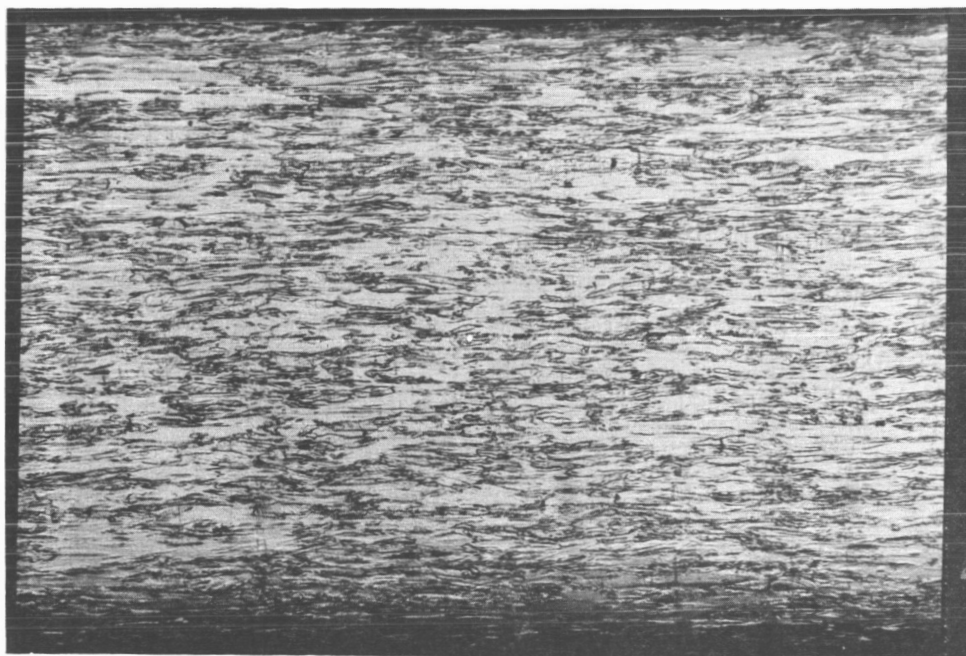
Carbon	65 ppm (parts per million)*
Magnesium.	2 ppm
Silicon.	2 ppm
Manganese.	1 ppm
Al, Cu, Ag	<1 ppm

Before mounting the specimens in the adhesion test apparatus, the wire was vacuum degassed for 2.5 hours at 1000°C at a pressure below 5×10^{-7} Torr. The resulting microstructure is shown in Figure 3. Hardness tests on a Scheffield Hardness Tester gave an average Knoop Hardness Number at 100g load of KHN 275 for the metal as received and KHN 75 for the outgassed metal. Hardness measurements after the adhesion experiments, e.g. several cycles of severe outgassing below 10^{-9} Torr, were unsuccessful because the metal had become too soft to give consistent results on the hardness tester.

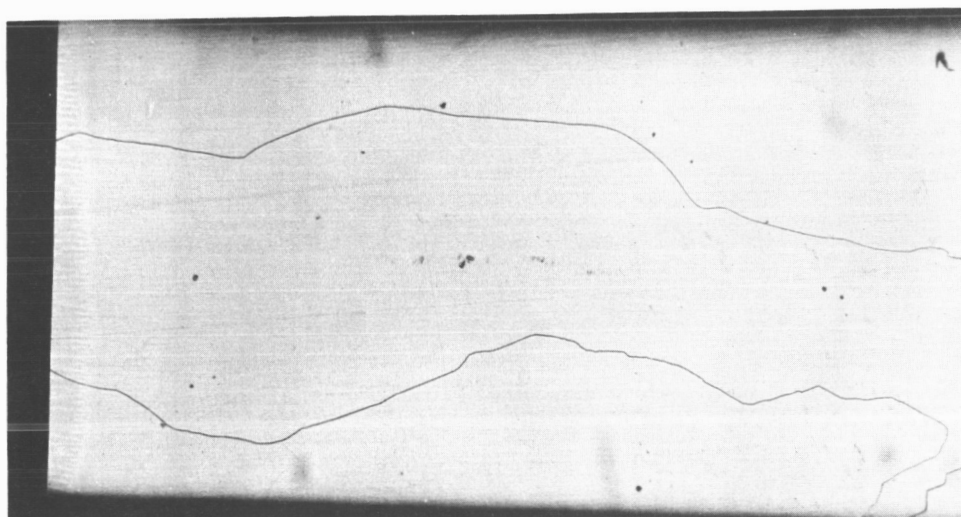
Apparatus

The vacuum system illustrated schematically in Figure 4 consisted of a Welch-Duoseal pump trapped to two CVC 2 inch Blueline diffusion pumps in series. The pumps used DOW 705 diffusion pump oil, and were separated from the diffusion cell by two 2 inch Granville-Phillips Cryosorb traps in series and a 1 inch Granville-Phillips UHV isolation valve. The liquid nitrogen trap adjacent to the diffusion pumps served as an oil baffle when the adhesion

* Analysis by National Spectrographic Labs



A. AS RECEIVED (100 X)



B. AS MOUNTED IN CELL AFTER OUTGAS (100 X)

FIG. 3 LONGITUDINAL MICROSTRUCTURE OF 99.993%
IRON - 65 PPM CARBON SPECIMENS

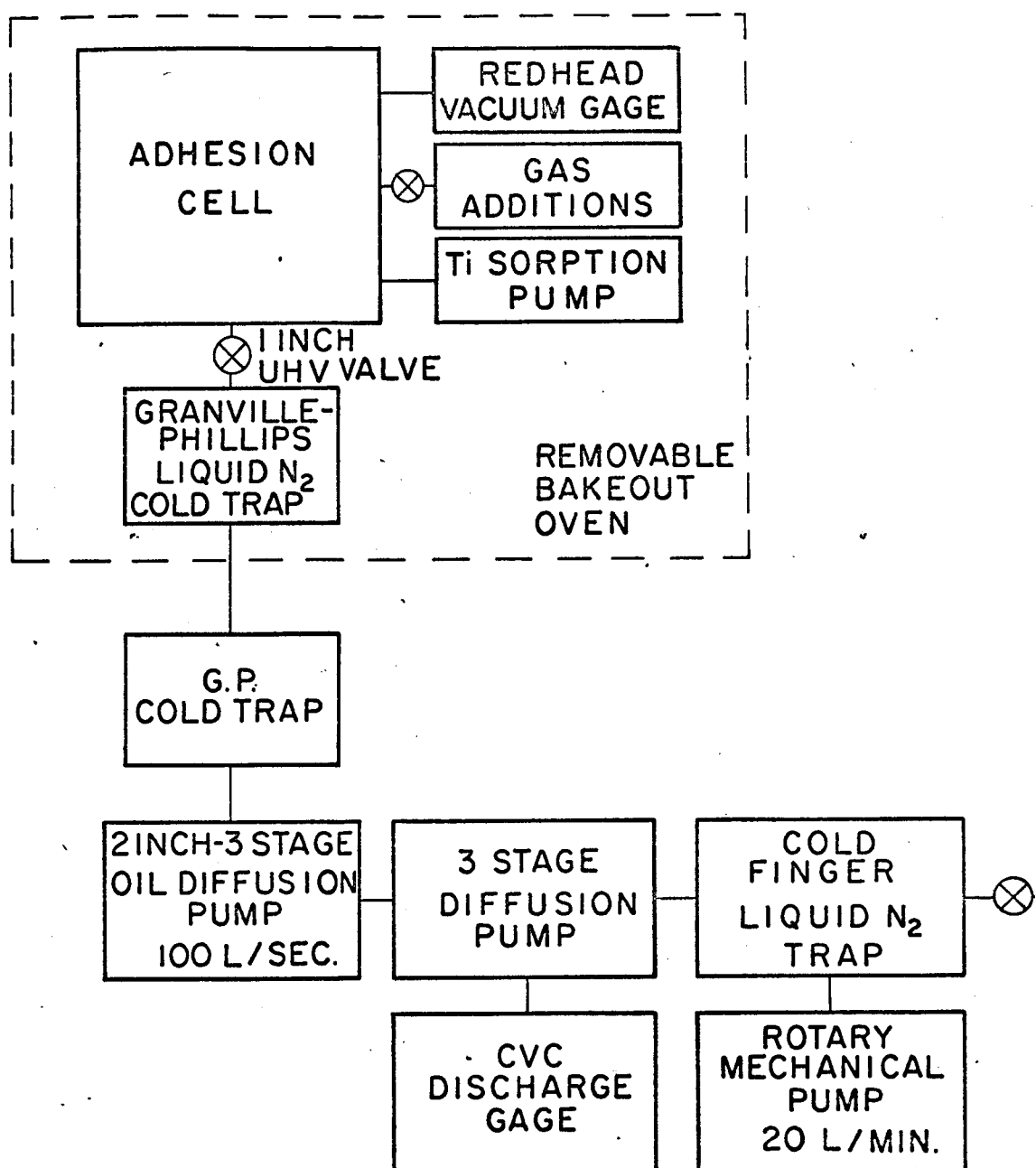
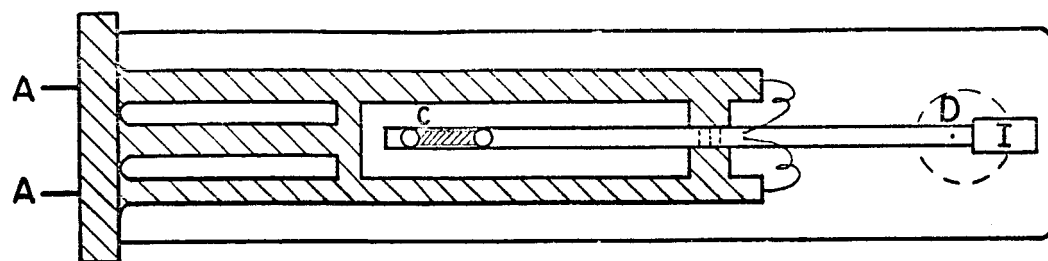


FIG.4 VACUUM SYSTEM

cell and second trap were subjected to a 10 hour bakeout at 450°C. Upon cooling the system after bakeout and placing liquid nitrogen in the trap adjacent to the cell, pressures in the adhesion cell below 10^{-9} Torr, and occasionally below 10^{-10} Torr, were readily achieved. The system pressure during bakeout was monitored by a GPH-100A cold cathode gage mounted in the foreline of the diffusion pump adjacent to the Cryosorb traps. Near completion of the bakeout cycle the foreline pressure was usually below the lowest gage division, e.g. 10^{-7} Torr.

The 50mm O.D. x 300mm pyrex adhesion cell shown in Figure 5 was affixed to the vacuum system isolation valve by means of a 40mm pyrex-metal conflat flange, which also supported side-arms for the titanium sorption pump and the argon gas supply. The titanium sorption pump consisted of a 0.25mm titanium wire wrapped on a 0.40mm tungsten wire, and then formed into a 1.50mm I.D. helix and mounted on the legs of a glass-metal electrical feed through. Upon thorough degassing and partial flashing of the wire immediately after bakeout, the small pump (50mm x 75mm length) could maintain the adhesion cell pressure below 10^{-9} Torr when the 1 inch isolation valve was closed to prevent oil contamination. The argon gas storage cells were isolated from the main system by a 0.5 inch Granville-Phillips valve. Several 20 cc pyrex storage cells were filled with spectrographically pure argon and isolated from the UHV system by glass break-off seals that could be broken with an iron slug when argon pressure was desired.

The pressure in the adhesion cell was measured by a Redhead Gage (NRC Type 752) mounted on a 25mm pyrex tube of low conductance and in line of



TOP VIEW - TORSION BEAM AND SUPPORT

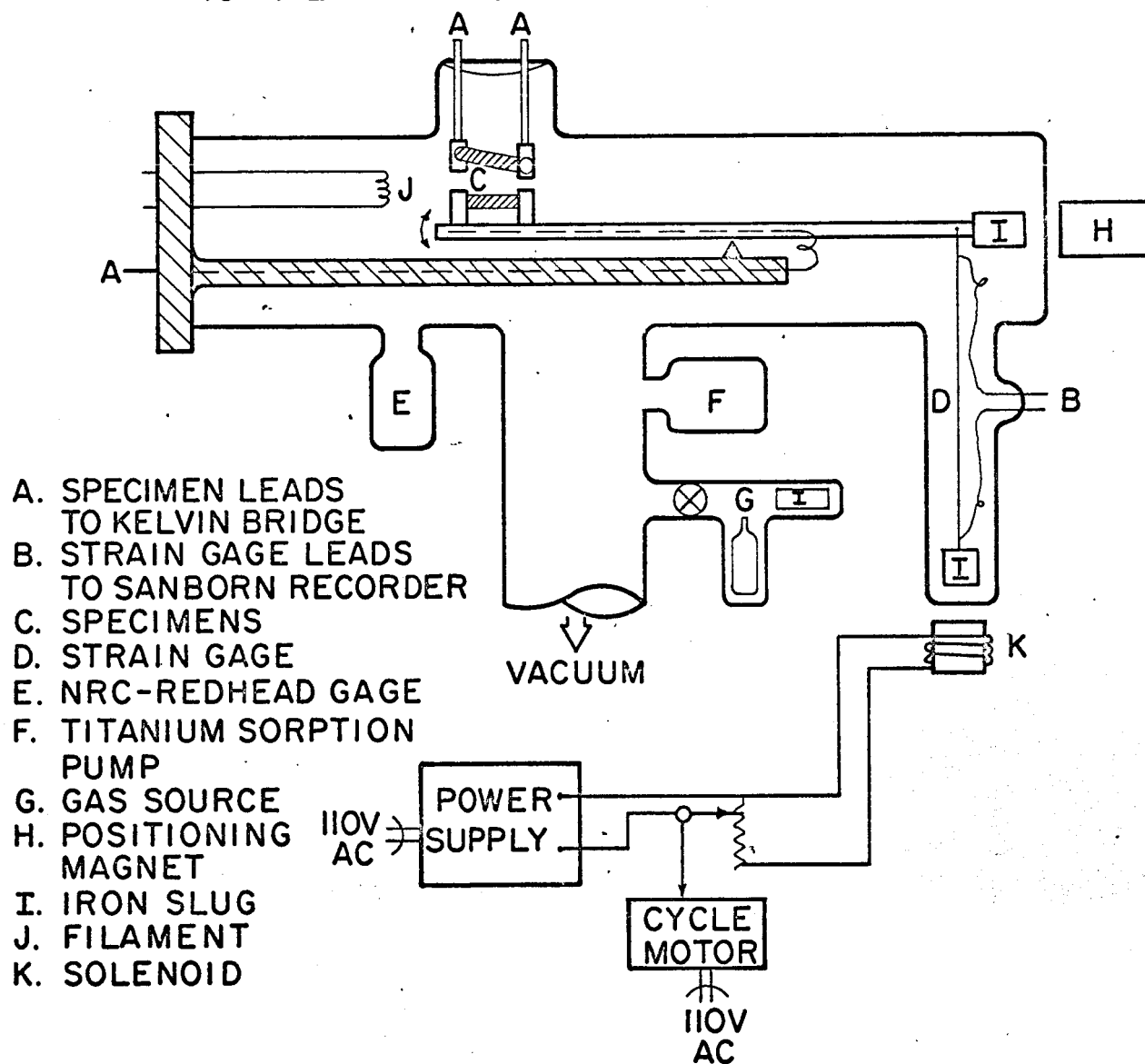


FIG.5 ADHESION CELL

sight with the samples.

The adhesion test apparatus consisted of two 1.5mm x 25mm iron wire samples fixed in the cell in a crossed configuration. One was attached to a glass-metal through seal by means of two alumina shielded molybdenum holders. The second sample was mounted on one end of a two hole alumina tube in the same type molybdenum holders. The alumina tube acted as a torsion balance and was supported by an aluminum bracket on a tungsten wire at the balance point. Two 5.0mm stainless steel support rods were welded to the conflat flange to support the tungsten wire between them in a horizontal position. The conflat flange also supported two 12.5mm pyrex-kovar through seals for filament leads and power leads to the iron sample mounted on the beam. A magnetic rod (I) was fixed to the torsion beam at the end opposite the sample. This magnetic rod allowed the torsion beam to be moved and thereby position the sample on the beam relative to the fixed sample. A maximum separation of about 30mm could be achieved during argon ion bombardment. Also fixed at the end of the beam opposite the sample was an isolated support wire for the 150mm nude 0.023mm constantan strain gage wire (D). The lower end of the strain gage wire held a second magnetic rod (I), through which a load was applied to the samples by a solenoid (K) outside the system. The external leads to the strain gage entered through a side arm mounted glass-metal seal.

The samples were brought into proximity during a normal adhesion cycle by adjusting an external permanent magnet relative to the magnetic rod on the end of the torsion beam till a few mm separation remained between the

two samples. In this configuration a load was applied to bring the samples into contact; at the end of the loading cycle this residual separation force was available to cause fracture if adhesion occurred. The load on the contacted samples was applied by varying the line input to an Electro DC power supply between zero and 110 volts, while the power supply output was set at a predetermined voltage corresponding to a solenoid field necessary to establish a peak load. This solenoid input power was varied by driving a variac with a synchronous motor which reversed at the 110 volt point and reduced the voltage linearly to zero. The load was applied and removed at a rate of 1.62 gms/min during a normal adhesion cycle.

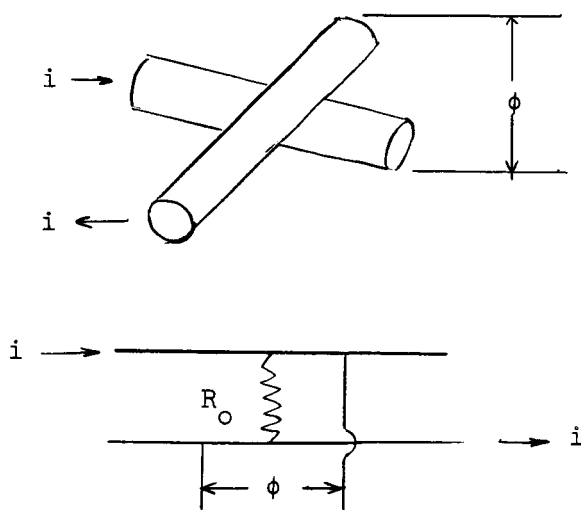
The strain gage detector consisted of a Sanborn-Model 312 transducer amplifier indicator with the smallest division in this system corresponding to 0.02 gms, readable to within ± 0.010 gms. After each series of adhesion runs the strain gage - mass relationship was calibrated through the 0-5gm range of operation by replacing the fixed upper sample with a calibrated force transducer. The readings of the strain gage amplifier were then compared directly to a known load. This eliminated any question of variables, such as beam flexing or friction, which could arise if the gage were calibrated after removal from the system or by other indirect techniques. The range of sensitivity of the mass measurement was found to be ± 0.010 gm.

Numerous studies were made of the automatic loading profile during the standardization procedure, i.e. when the standardized force transducer replaced the fixed sample. This was accomplished by placing the output from the Sanborn 312 transducer amplifier as the input to the "y" function of

an "x - y" recorder, and following the cyclic variation with time. The load was applied in a near perfect sawtooth curve with a slope of 1.42 gms/min. No significant variations from this shape were encountered.

The torsion beam arrangement was designed for pure normal loading. The object being to reduce shear deformation in the interface of the adhesion couple to a minimum during loading, since small tangential movement can rupture the contaminant films. The only tangential motion arose from very small, but unavoidable vibration. Under very light loading (<30 mg) and non-adhesive conditions, these vibrations could be observed as an instability in the contact resistance reading.

The circuit diagram for the measurement of contact resistance (R_o) is shown in Figure 6. Crossed-wire contact of the samples is illustrated below to show how the current (i) provided from a 0.006 volt open circuit source, passes through the contact resistance (R_o) to produce a potential drop (ϕ).



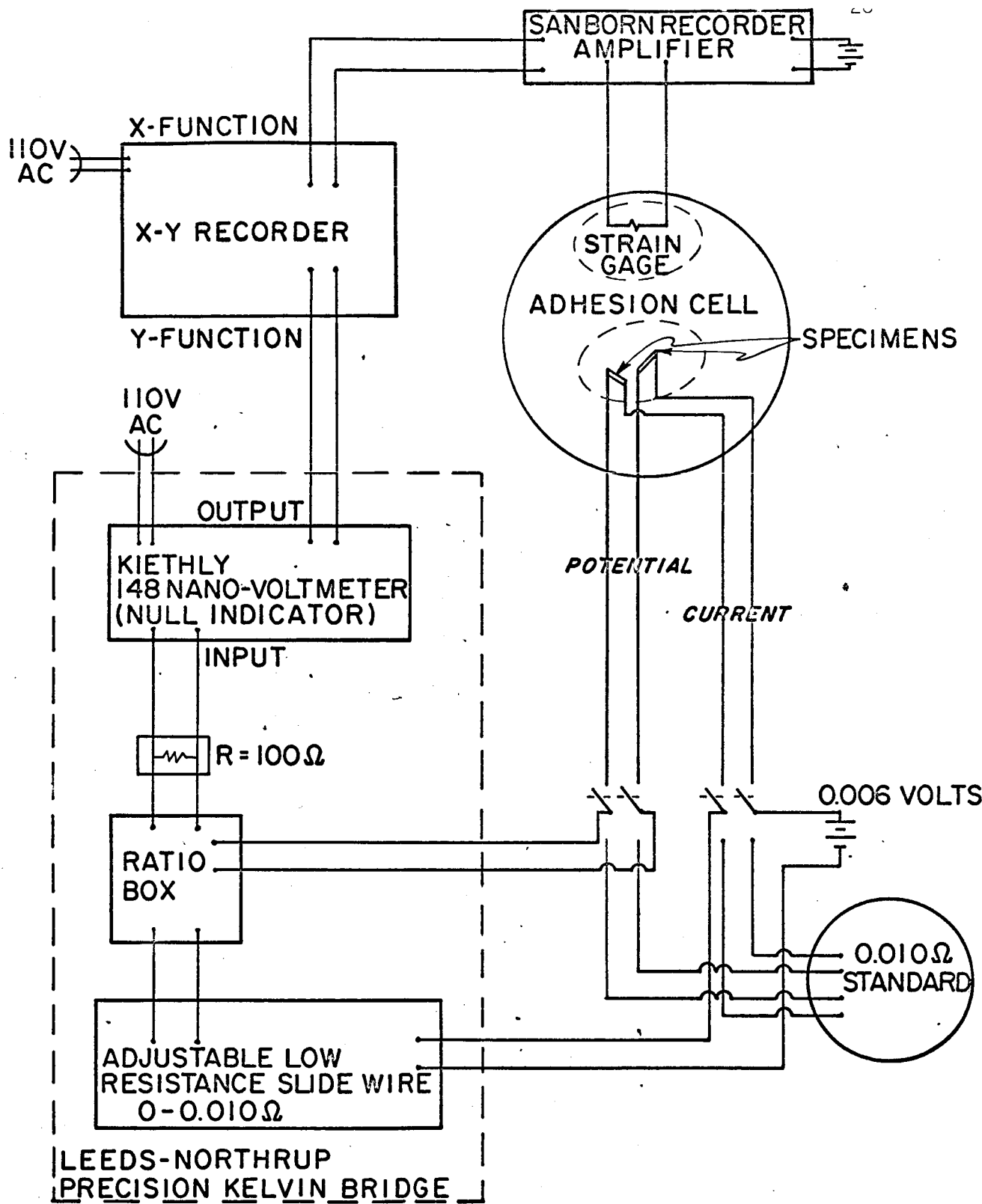


FIG.6 RECORDING CIRCUIT.

This four point resistance contact was placed in a Leeds and Northrup Precision Kelvin Bridge as shown in the circuit illustrated in Figure 6. The bridge, a secondary standard for measuring resistance, was standardized prior to each run with a primary NBS standard of 0.010Ω . The potential drop across the sample was compared to that across the bridge with a Kiethly 148 Nanovoltmeter as a null point indicator.

In order to use the output of the Kiethly as a measure of contact resistance variation and as the input to the "y" function of the "x - y" recorder, the maximum load point, i.e. the minimum R_0 point, was first established. This was accomplished by placing the samples in contact at a particular load and then balancing the Kelvin Bridge to the null point. The "y" function of the "x - y" recorder was then calibrated so that the point $y = 0$ corresponded to the null point. Nanovoltmeter sensitivity and the corresponding value of the deflection of the null indicator was determined by setting the scale range, i.e. full scale in decade steps each giving a different value to the point $y = 10$. The full scale range of deflection for the various settings was:

1 μv range	0.045 Ω
3 μv range	0.160 Ω
10 μv range	0.500 Ω

For example, if a voltmeter sensitivity of 3 μv was used, a change in contact resistance of 0.01Ω corresponded to about 1.5 cm in the "y" function distance.

This technique was standardized by replacing the contact resistance of the samples with a secondary standard which could be varied in 0.01Ω steps. The "y" function plot-out could then be directly related to the variation of the standard. Under normal conditions the most sensitive scale setting, i.e. $0.1 \mu v$ scale, represented approximately the third significant figure in the milliohm range or $\pm 10 \mu$ ohms.

The "x" function represented the output of the Sanborn 312 Amplifier from the calibrated strain gage, cf. above, and indicated the load placed on the samples.

A standard adhesion run was initiated after the samples were placed within a few mm of each other, by activating the drive motor of the automatic loading solenoid. In place of the Kelvin Bridge System, an external circuit capable of detecting very high resistances, was utilized to detect and record the instant of sample contact or zero load point. As loading of the samples continued, the Kelvin Circuit was switched in through a heavy knife blade switch and R_0 recorded versus the applied load to the peak load. Since the sensitivity of the null point circuit limited the following of very high resistances, occurring under extremely light loads, e.g. less than 0.5gms, this region of the "x-y" plot was not recorded. Presently this information is not considered to be of significant technical value as is discussed below. During the unloading cycle the high resistance measuring circuit was again switched in and the sample separation point compared to the contact point to insure that drift in the load circuit was negligible.

The contact creep curves, discussed in the next section, were plotted by replacing the "x" function with a time sweep, 0 to x = 60 seconds. The samples were brought into instantaneous contact at a fixed load by switching a known current into the solenoid. Changes in contact resistance were then plotted for a period of two to three minutes. Several curves of this type were prepared under various loads and conditions at room temperature.

Procedure

The outgassed iron samples were mounted in the cell and the system evacuated to a pressure $<10^{-5}$ Torr, at which point a series of adhesion cycles were conducted at various loads. The bakeout cycle was then initiated. After cooling from 450°C , filling the upper trap with $\text{N}_2(1)$ and outgassing the various components, the pressure was usually about 2×10^{-10} Torr. An additional series of adhesion cycles were then performed.

As indicated by previous workers, it is necessary to conduct a series of adhesion cycles at each major change in operating conditions. This will assure that the contact resistance apparatus is operable and performing in the predicted manner, i.e. as the surface contaminants are removed the value of R_0 decreases substantially, cf. Saunders (56). Secondly, this will detect bulk adhesion at any of the intermediate stages; a phenomena which has not normally been observed until after the surfaces are argon ion bombarded. An additional resistance heating was carried out at greater than 1000°C for about one half hour for each specimen, till pressure was $<10^{-7}$ Torr at temperature. The titanium sorption pump was then flashed

to maintain the pressure at approximately 10^{-10} Torr which prepared the system for argon ion bombardment.

Ultra high purity argon was admitted into the system to a pressure of about 10^{-4} Torr by breaking a capsule tip and slowly opening the leak valve. A DC potential of one Kv between the specimens, with 2 ma current, initiated ion bombardment. After each sample was bombarded for about two hours, a small nickel shield was placed (with a magnet) between the samples to shield the sample not being cleaned from sputtered material during an additional half hour cleaning. The potential difference was established with a filament (Figure 5). A considerable deposit of sputtered material on the cell walls attested to the removal of a substantial amount of surface material during the cleaning process.

After this phase, the argon was evacuated and both samples annealed above 1000°C for about an hour each to minimize surface damage and desorb argon from the surficial layers. Adhesion cycles were performed after each of these stages of surface cleanliness. Additional argon cleaning and anneal treatments were conducted before each new series of tests or if several hours had lapsed between phases of one run.

Over 150 adhesion cycles were recorded for the iron - 65ppm carbon couple. As mentioned, tests were made for different stages of surface cleanliness, loading rates were constant, and the changes in the system were recorded continuously.

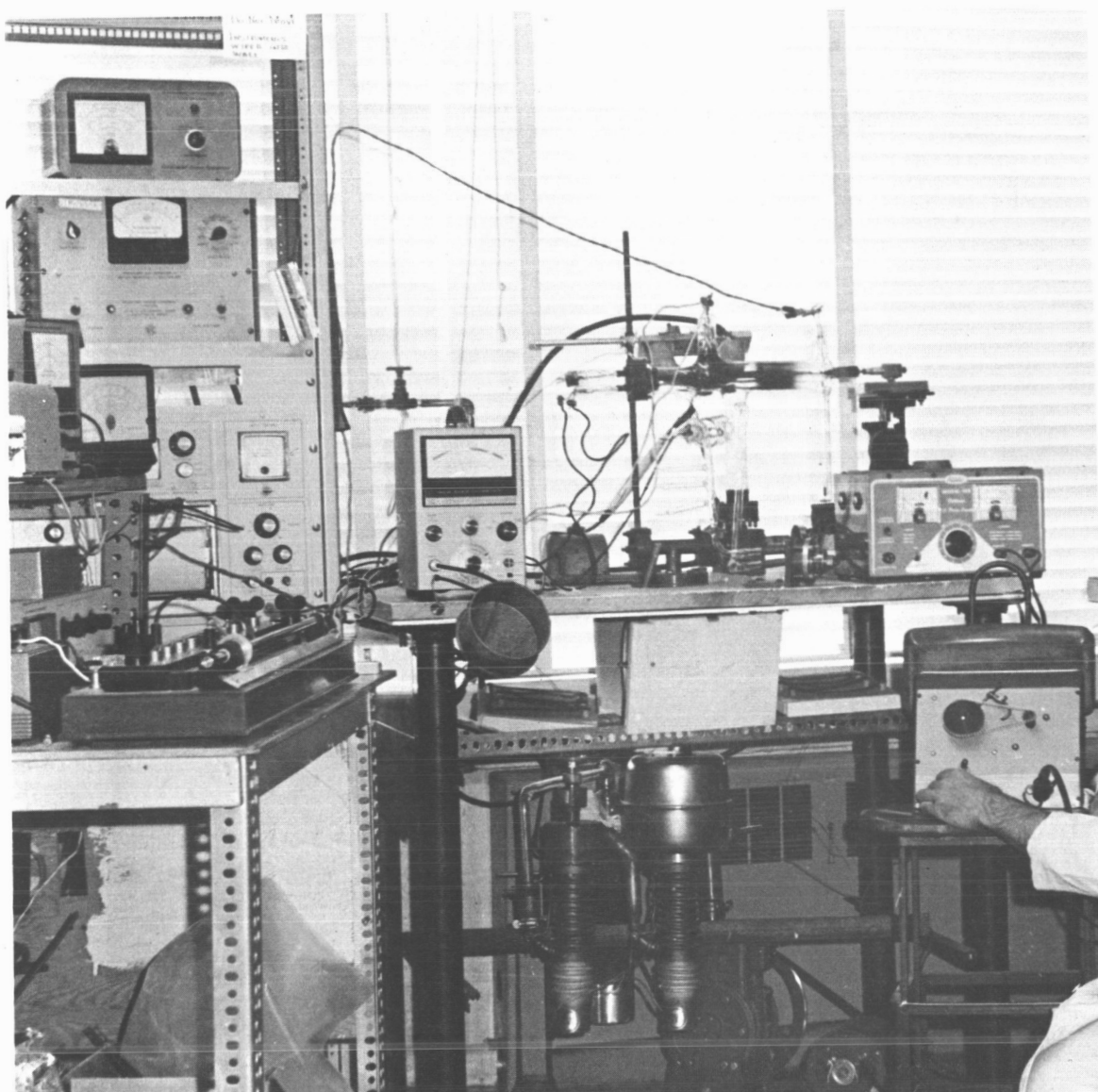


FIG. 7 ADHESION TEST APPARATUS

III. RESULTS AND DISCUSSION

The experimental technique was basically the same as that discussed previously by Johnson (20) and Saunders (56) except for automatic loading and unloading techniques and the continuous recording of the data, R_o versus W , with the x-y recorder. The results were extracted from over 150 adhesion cycles under different surface and loading conditions.

Contact Resistance

Continuous recording of an entire adhesion cycle provides distinct advantages towards a better understanding of the mechanism of adhesion through the recording of R_o versus load (W) as a continuous undisturbed process. As a consequence, a more comprehensive picture is presented of the deformation, adhesion and fracture of asperity junctions, formed between two metal surfaces in intimate contact.

Previous experiments indicated that adhesion of ultra clean metals can be distinctly characterized by the shape of the R_o versus W curve. If the unloading curve reproduces the loading curve, gross adhesion was not involved in the interface formation. If, however, R_o remained constant during the unloading cycle as is shown in Figure 8, adhesion of the interface layers was involved.

These effects were fully discussed in the previous studies (19,20,56) of the couples Ag-Ag, Mo-Mo, Ti-Ti, Ag-W, Ag-Ni, and Cu-Ni for both clean and contaminated states. This investigation verifies and extends these observations, with the continuous recording apparatus, for the system iron-65ppm carbon. The investigation is also unique in that the effects of a bulk contaminant, carbon,

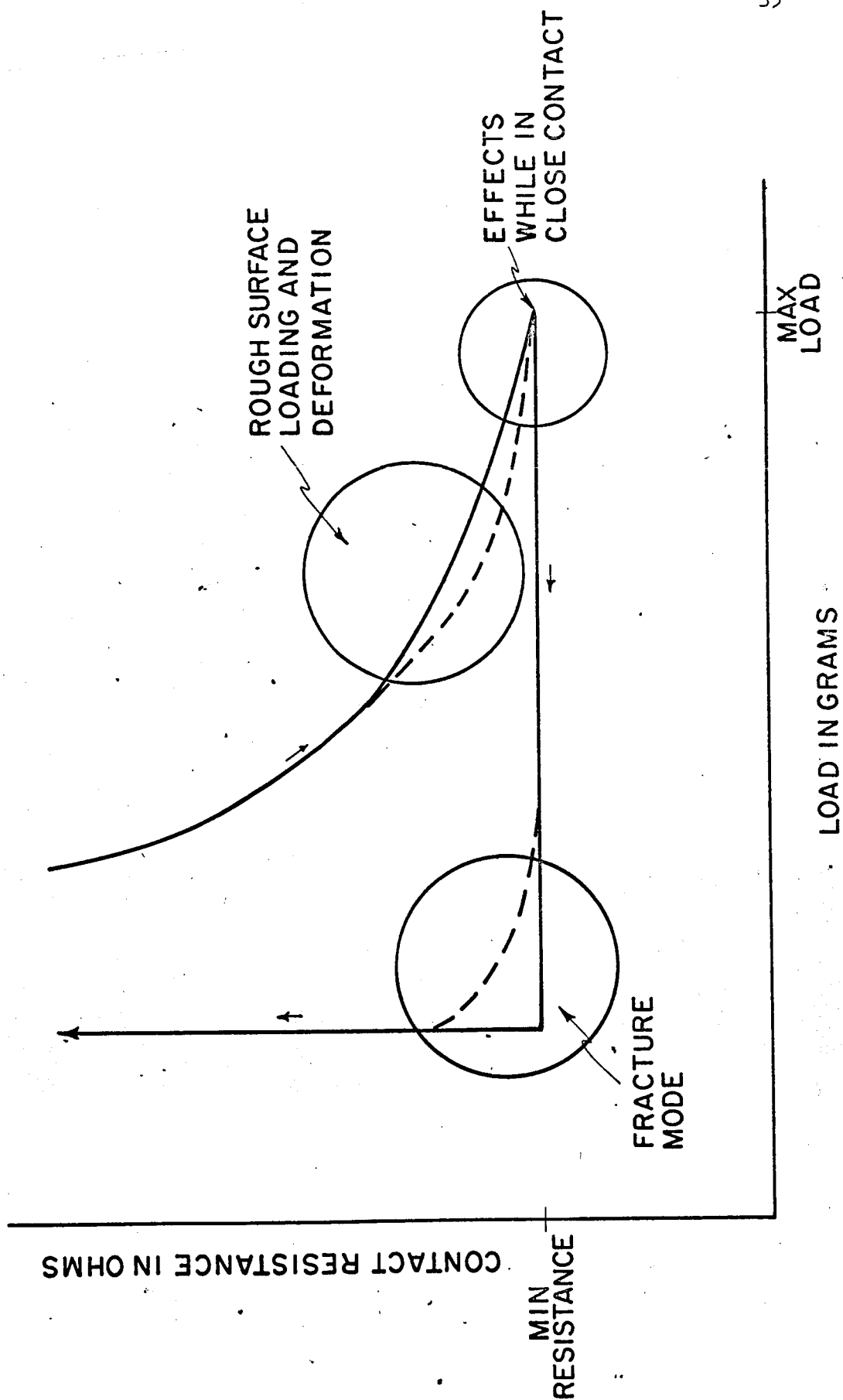


FIG.8 INFORMATION FROM CONTINUOUS ADHESION PLOT

are evaluated in detail; as a consequence no details of the effects of gaseous contaminants were recorded. Creep phenomena in the contact area under constant load was also shown for the first time by recording R_0 over a period of time after the instantaneous application of the load.

Figure 9 is a direct reproduction of an "x-y" plot in which R_0 ("y" function) is plotted versus load ("x" function) cycle. Prior to the cycle shown in Figure 9, the surfaces were each exposed to several hours of ultra high vacuum (UHV) degassing, argon ion bombardment and UHV annealing above 1000°C . Surface oxides and other atmospheric contamination were completely removed, and therefore, nearly atomically clean iron surfaces would have been present provided no bulk contaminant was present in the system.

The power relationship between R_0 and W as expressed by equation 11 suggests that the character of the deformation process can be best represented by a plot of $\log R_0$ versus $\log W$ as shown in Figure 10. Figure 10 also indicates the reproducibility of the experimental technique since the series of runs 30 - 33 was conducted on the same contact spot with about the same load. A sufficient number of similar series were made at different contact spots to permit this group to be called a typical series. The reader is reminded that the events at the interface contributing to the characteristic shape of the plot involve numerous asperities of sub-micron dimensions and a nominal contact radius of a few microns (10^{-4}cm). The log-log plots were extracted from continuous "x-y" plots as shown in Figure 9 and, as a consequence, the datum points represent only significant points selected from the continuous curves.

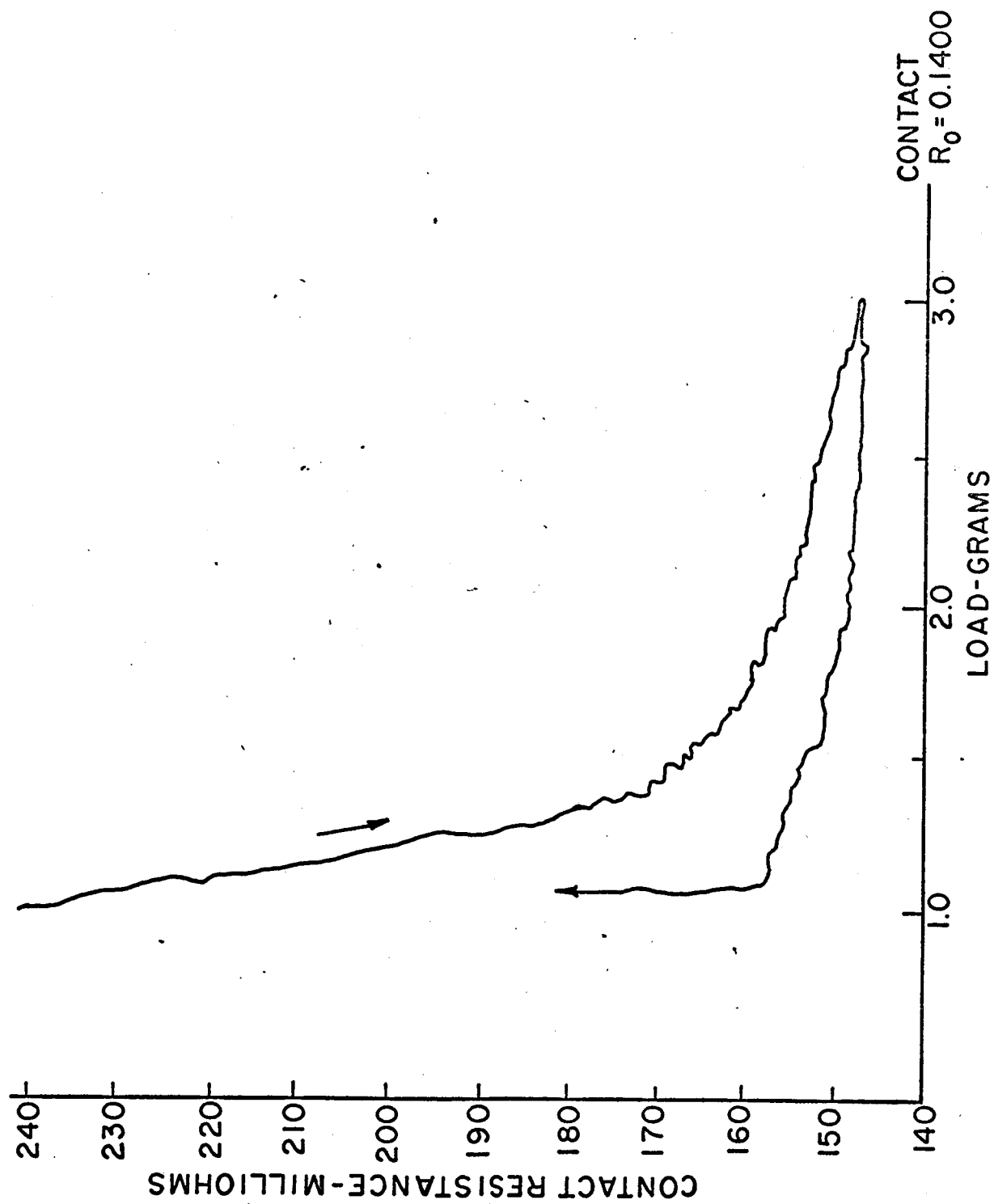


FIG. 9 TYPICAL "X-Y" PLOT FOR IRON - 655 PPM CARBON ADHESION CYCLE

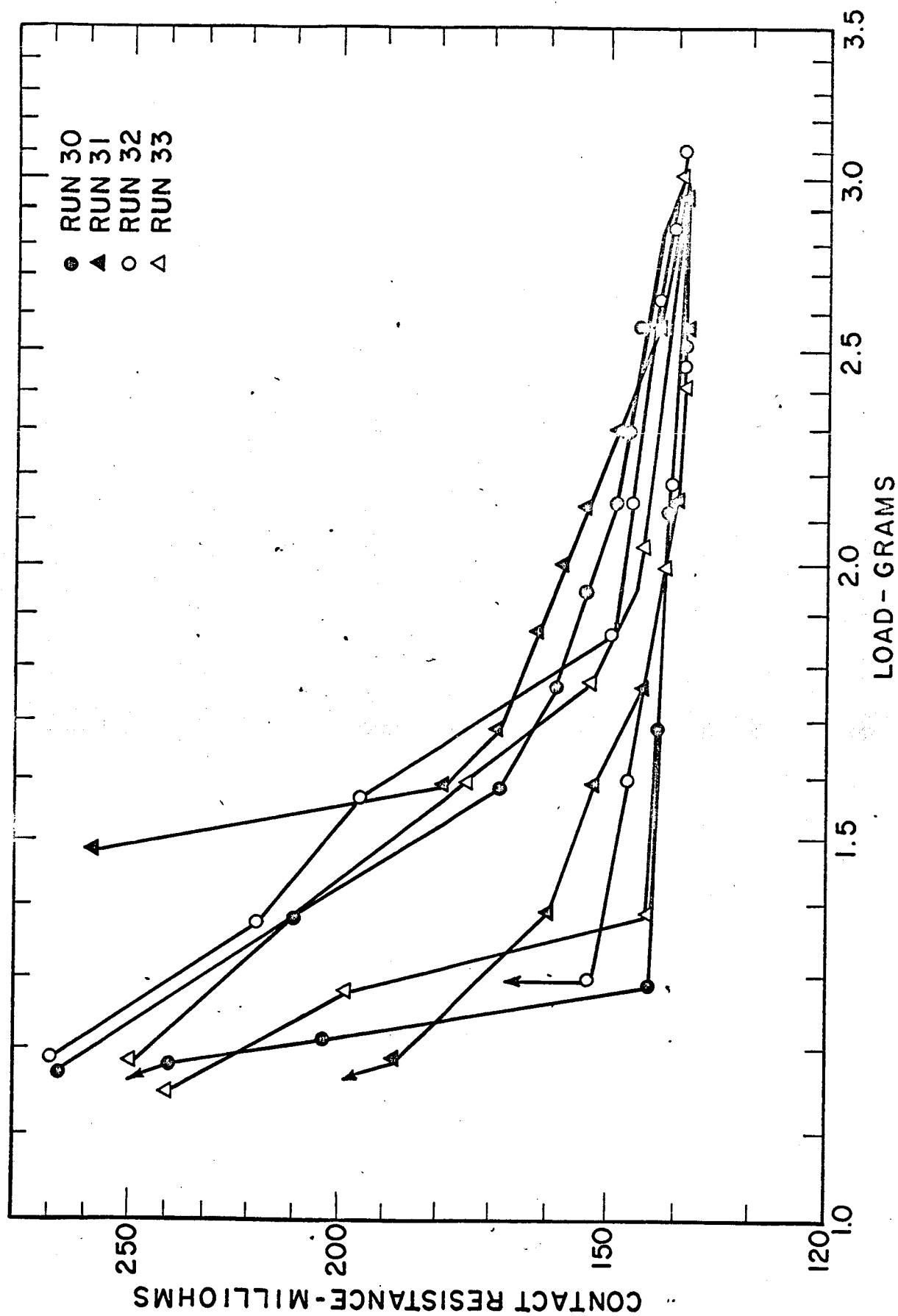


FIG. 10 TYPICAL ADHESION CYCLES BETWEEN IRON - 65 PPM CARBON COUPLES ON THE SAME CONTACT POINT

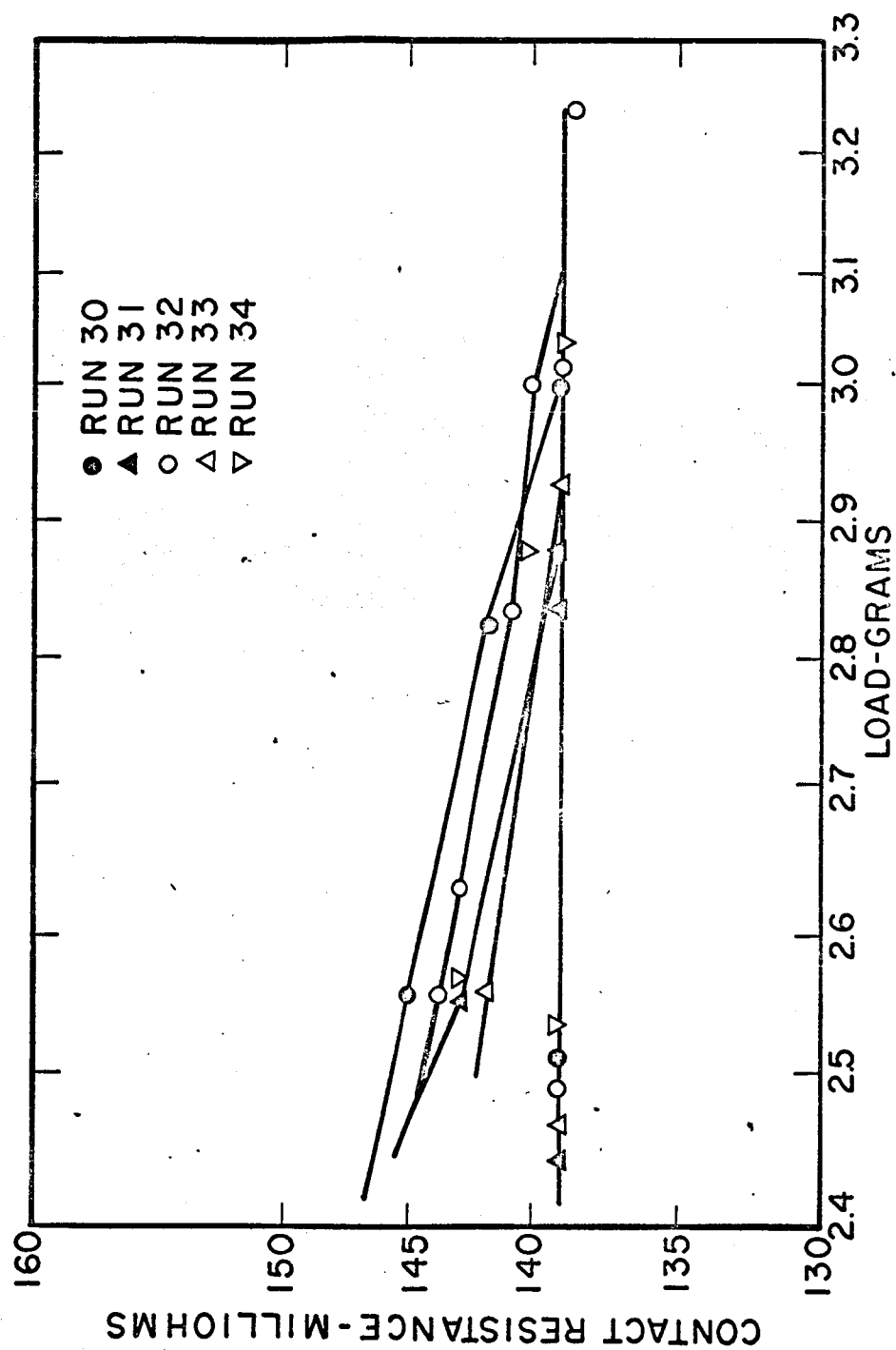


FIG. II EXPANDED SCALE OF FIG. 10

A number of significant features ought to be considered in the characteristic shape of the runs 30 - 33. The deformation process at light loads seems to have a slope (log-log plot) in the range of -2 which changes to about -0.4 as the load is increased to about 1.6 - 1.7 gms. At some point greater than 2.5 gms the slope again changes, here the value is -0.15 or less. The degree of scatter can be shown approximately

Stage I -2 ± 0.5 slope

Stage II -0.4 ± 0.1

Stage III -0.15 ± 0.05

These same stages seem to be characteristic of a number of different series.

During unloading R_0 remains constant to a point of about 1.3 grams contact force, at this load the stable junction disintegrates to a contact resistance value approximating the loading value of R_0 as measured during the loading cycle. This aspect will be discussed later based on the load deformation mechanisms.

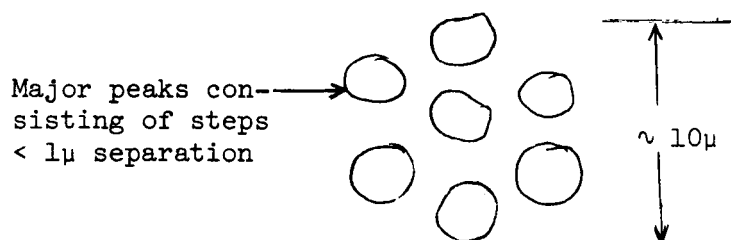
Let us first examine the role played by the surface irregularities during the deformation process. The term, n , the number of contact points, cf. equation 11

$$n^{1/4} R_c = 6.3 \times 10^{-3} W^{-1/2}$$

will vary with W in an unknown fashion; intuitively however, and in the light of Williamson's recent work, it is reasonable to assume that n increases rapidly from one asperity at contact under extremely light loads to a rather large constant value. The constancy of n at heavier loads seems to be a reasonable approximation since the number and size of

the surface asperities are usually distributed in a Gaussian form. As the highest asperities' radii are expanded, they will bring into a common contact area the adjacent satellite asperities at a rate approximately equal to the rate that the central depression areas of the apparent contact region are expanding and including new asperity contacts. If the previous assumptions are consistent, the value of the $\log R_o$ will become directly proportional to the log of W when n becomes constant. This suggests that the slope of the $\log R_o$ versus $\log W$ plot is related to the deformation mechanism of the asperities.

From a series of carefully prepared photomicrographs at 600X the surface of the Fe-65ppm C samples after the series of experiments, and average model of the asperity concentration was constructed as shown:



If one assumes that 3-5 steps will be involved in each major peak, then the number of contacts (n) under a light load, will range between 20 and 35. With this information let us consider the possible variations of $R_c = R_o$ for the iron-65 ppm carbon system when loaded under the terms and constraints of equation 11. Four hypothetical curves of $\log R_c$ versus $\log W$ are shown in Figure 12 and are plotted under the following limits:

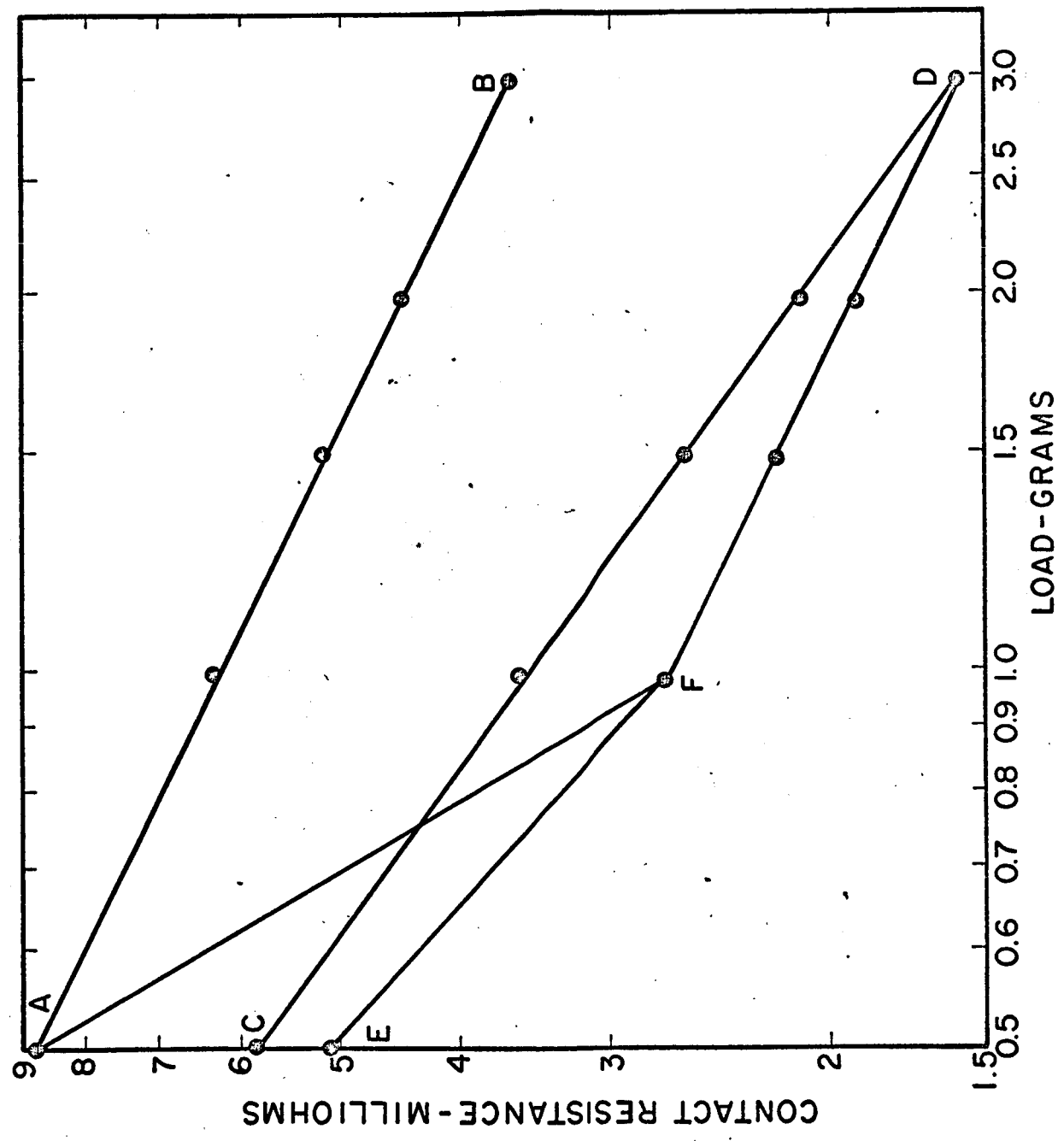


FIG. 12 THEORETICAL CURVES UNDER VARIOUS CONDITIONS OF MULTIPOINT CONTACT. CF. TEXT FOR EXPLANATION

- A - B Single point contact throughout loading: $n^{1/4} = 1$
- C - D The number of contact points continuously increases with load: at 0.5 gm, $n = 5$; 1.0 gm, $n = 10$; 1.5 gm, $n = 15$; 2.0 gm, $n = 20$; 3.0 gm, $n = 30$.
- E-F-D The number of contact points varies as: 0.5 gm, $n = 10$; 1.0 gm, $n = 30$; thereafter $n = 30$ constant
- A-F-D The number of contact points varies as: 0.5 gm, $n = 1$; 1.0 gm, $n = 30$; thereafter $n = 30$ constant

The curve A-F-D represents most closely the conditions expected in the experiments; however, one should note that the point at which n becomes constant was arbitrarily chosen as one gram.

A comparison of the theoretical curve shown in Figure 12 is made with run 30 from Figure 10 in Figure 13, where afdd' is a reproduction of the observed run 30. Also plotted on Figure 13 is a curve A'F'D which represents an order of magnitude displacement of curve A-F-D to a higher resistance. For now, this displacement can be considered as simply the change in bulk resistivity of the iron concerned from $9.7\mu\Omega\text{-cm}$ to $97\mu\Omega\text{-cm}$ which will account for the two curves. Further explanation for this change will be developed below. Since the shift in position of A-F-D to A'F'D' does not effect the slope of the theoretical curves, let us compare these with the observed curve afdd'.

The slope of the theoretical curve between A-F is approximately -2 or that of the observed data between a-f; furthermore, very high slopes were observed under light load for nearly all of the 150 runs conducted

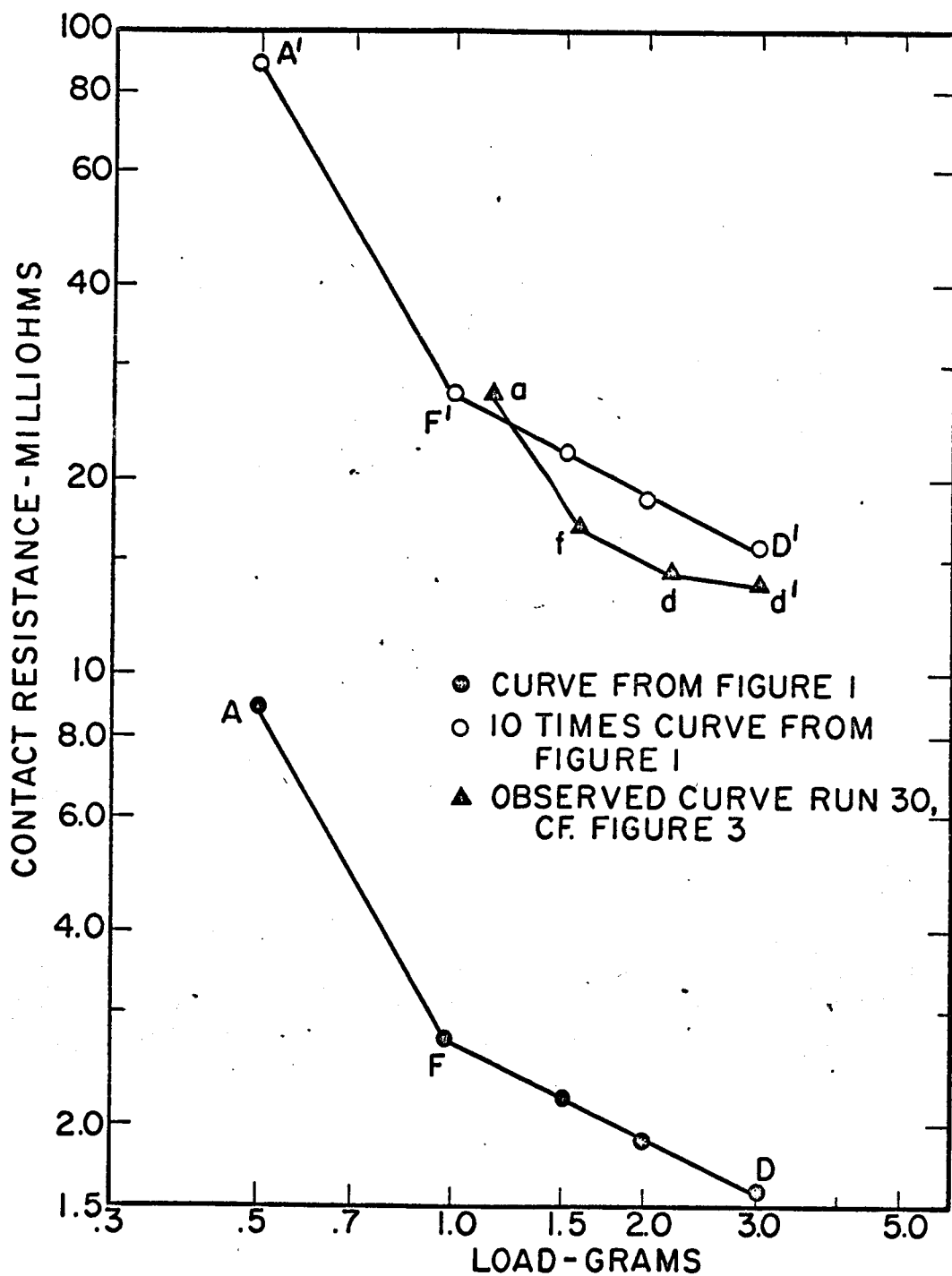


FIG. 13 THEORETICAL R_c VERSUS W CURVES AFD AND A'F'D' ARE COMPARED TO OBSERVED CURVE afdd'

in this investigation. Since the change from a few asperity contacts (A') to many (F') was arbitrarily chosen as 0.5 gms and 1.0 gms, this could also have been chosen to coincide with the observed curve (a-f). The slope between fd on the observed curve lies in the range -0.4 which is somewhat less than predicted in F'D'(-0.5). From the previous equations and the discussion of Figure 12, it is evident that if the number of asperities in contact is increasing, the deformation slope will increase in a similar manner. Since the observed slope (f-d) is less than that calculated at 0.5 and is linear, the difference cannot be attributed to a continuous change in the number of contacting asperities. Since resistivity does not vary significantly with pressure (71), the variation between f and d might be accounted for by breakthroughs in a contaminant layer; however, such breakthroughs would abruptly decrease the contact resistance also causing non-linear increase in slope, again not in accord with that observed. Variation in the yield point could shift the curve in the proper direction; however, one would expect a loss in linearity which is not observed.

The three most likely explanations for the smaller slope are:

- a. That the deformation process of the asperities is a mixture of elastic (slope -0.33) and plastic (slope -0.50) processes.
- b. That surface creep is superimposed on the deformation curve.
- c. Surface contaminants have modified the deformation process.

Creep has been observed to expand the contact area over a significant period of time, as is reported later in the discussion of Figure 15.

The small slope observed between d and d' is also a characteristic observed in Figure 10. Stage III may signify the beginning of bulk phenomena, i.e. where the interaction between asperities has ceased except for creep and bulk elastic support of the load has ensued. It is interesting to note that the slope of the creep curves shown in Figure 15 varies between 0.05 and 0.18 depending on the work hardening of the area tested. The slope of the last portion of the adhesion curve (Figure 10) also varies between 0.05 and 0.15.

Adhesion

Three criteria for metallic adhesion have been established (37):

1. A load approaching the fracture strength of the weaker material is required to fracture the samples.
2. The minimum contact resistance observed at maximum load on the couple is constant with unloading to, or very near to, the point of junction failure.
3. The contact resistance values are stable even under extremely light loading.

These criteria were not met by the majority of the adhesion cycles performed during this experiment as shown by those presented in Figure 10. It is evident from these curves, if we accept the second criteria as being significant, that fracture usually occurred at about 1.3 gms compressive load.

Previous workers (2) have postulated an inherent build-up of elastic stresses which are recovered by the system upon release of the loads, however, studies by Johnson (19,20) and Saunders (56), and the proposed experimental

model (cf. Section I) suggest that pure metal-metal contact does not permit the loss of any elastic stress by a reduction in contact area. In this light, let us examine a possible mechanism for producing the curves shown in Figure 10. As the load on the junction passes the maximum point and begins to slowly decrease, the energy to spring-back, or to release the elastic stresses, is accumulated along the interface. A stable interface, e.g. ultra pure metals, survives the full unloading cycle and R_0 is constant. With a brittle phase in the interface that cannot support the released elastic stresses, fracture will take place at a load representing sufficient energy build-up; even though the system is still under compression. When extremely weak adhesive forces are present in the interface, the unloading curve superimposes on the loading curve as previously discussed.

The latter can be considered to be an extreme case of our observations with the relatively clean surfaces of this investigation. The model which considers the existence of a brittle phase at the interface can be related to only one impurity, carbon, since there are insufficient other impurities present to form a monolayer. Contamination from either the gas phase or surface creep was ruled out since over 20 argon ion bombardments and UHV anneals were performed on the system between test series which did not appear to alter the results.

Let us examine the metallurgy of the system and additional evidence for the case of carbon as the most likely suspect for contamination. The solubility of carbon in pure α -iron varies with temperature as follows (64):

<u>T°C</u>	<u>ppm carbon</u>
723	950* (eutectoid temperature)
713	900
606	430
534	230
468	130
RT	10

*0.02 weight percent carbon

Upon cooling an ultra pure iron-carbon alloy at any carbon concentration greater than 20 ppm carbon and less than 950 ppm carbon from the annealing temperatures of the experiment, i.e. $> 1000^{\circ}\text{C}$ at a cooling rate of less than $0.3^{\circ}\text{C}/\text{sec}$, to room temperature, where the adhesion experiments are conducted, a precipitate of Fe_3C or Fe_2C would be generated as the maximum solubility limit is exceeded. The final system will consist of $\alpha\text{-Fe}$ grains with less than 10 ppm carbon in solution since the very slow cooling rate would most probably permit conditions very close to equilibrium to prevail, and the carbide precipitate which forms in the sub and grain boundaries as well as in free surfaces. The kinetics and morphology of this precipitation process at carbon concentrations between 600-900 ppm carbon have been carefully studied by several investigators as is conveniently reviewed by Christian (65) and Hume-Rothery (64). The precipitate nucleates in the internal and external surface regions principally because these regions offer the least resistance to the strain developed in the lattice as the new particle grows, e.g. the free energy is less because lattice strain is less in these regions of crystal disorder.

The free energy driving force to form the carbide particle at the interfaces far exceeds the energy driving force to permit the particle to redissolve in the matrix after a certain critical embryo diameter (micro-precipitate particle) is achieved (65); as a consequence, "uphill" diffusion in second phase transformation kinetics is a most common phenomena. By "uphill" diffusion (65) we mean diffusion against a concentration gradient such as 65 ppm carbon-iron forming carbide particles which are 25 A/o carbon. (250,000 ppm carbon).

In an alloy of 65 ppm carbon-iron, the volume percent of carbide is less than 0.01% and as a consequence pearlite colonies as observed eutectoid steel (36,100 ppm carbon) would not be expected to be observed since the colonies are a product of the eutectoid reaction (duplex growth, or precipitation) rather than general precipitation as described above (65).

Martensite has been observed (66) in iron containing 100 ppm carbon; however, this material is only prepared if the quenching rate exceeds 3.5×10^4 deg C/sec. Since our equipment permits only 0.3 deg C/sec, little concern over the presence of martensite has been made.

The time-temperature relations which are necessary to allow carbon to diffuse to an external surface of the system are also important. Since the diffusion distance of carbon in iron is approximately related to the \sqrt{Dt} , where t is the exposure time and D is the diffusivity which is at least 10^{-6} cm²/sec at 1000°C (64), an estimate of the time it would take to diffuse a carbon atom from the center of the wire sample (0.15 cm OD) to the surface under a 1000°C anneal would be approximately 1.5 hours. As pre-

viously indicated, the conditions of anneal were more rigorous than this conservative estimate since longer times were employed at higher temperatures.

In conclusion, the metallurgical factors which would place a higher concentration of carbon in the surficial layers, i.e. carbides Fe_3C (250,000 ppm carbon) or Fe_2C (330,000 ppm carbon) of an iron sample containing 65 ppm of carbon, appears to be consistent with the proposed observation.

Drs. P. Sewell and D. Mitchell of the chemistry branch of the National Research Council of Canada (67) claimed in a recent discussion to have positive high energy electron diffraction (HEED) (Ultra High Vacuum) evidence that carbon will concentrate in the surface layers of ultra pure iron with carbon concentrations below 100 ppm. Although the ultimate test, i.e. utilizing the HEED with an x-ray analyzer, has not yet been employed on iron, the evidence from extremely careful electron diffraction studies leaves no doubt in their mind as to the presence of excess concentrations in the surface. The strength of their observations was magnified by the observations of Drs. D. Kaplan and R. Hussy of the same laboratory (68) studying 1000 ppm carbon-iron which was subjected to a 700°C hydrogen treatment by an ultra high vacuum degas which permitted what was called a "massive" overgrowth of Fe_2C to form at the surface at the expense of sublayer decarburization. The crystal structure of Fe_2C was positively identified by electron diffraction and the decarburization of the layers immediately below the surface by optical techniques. The presence of surface excess concentration of carbon has also been observed and identified in

several other transition metals including tungsten and molybdenum. Since these studies, for the most part, were conducted under extremely ideal conditions, e.g. ultra high vacuum ion pumped system, by well established surface researchers, it was generally assumed that the carbon originated from within the sample, similar to the case of tungsten (42) where the proof is most readily attained by flashing the metal to 2000°K in the presence of oxygen and monitoring the increase in carbon monoxide concentration in the system by mass spectrometric techniques and regenerating a carbon surface by annealing.

The first crystals of iron prepared for Drs. A. Pignocco and G. Pellisier (69) of U.S. Steel for use in their low energy electron diffraction (LEED) experiments were accidentally contaminated with 200 ppm carbon from a carbon filament furnace. The resulting LEED patterns were most complex and could not be related to either α (body centered cubic) or γ (face centered cubic) iron crystals even through extensive argon ion cleaning; concentration was detected, however, when a crystal of less than 10 ppm carbon was substituted, the proper respective crystal patterns were observed and the original oxidation study undertaken. In the first 200 ppm carbon atoms statistically distributed in an iron surface would not interrupt a normal LEED reflection pattern expected from a crystal of iron as discussed by MacRae (32); therefore, it must be assumed that the material present in the surface which causes a complete loss of the iron crystal is present in a very high concentrations and is most probably carbon in the form of carbides.

It is a relatively simple process to illustrate why Pignocco indicated that little or no problem with surface carbon concentration was observed when the bulk concentration of carbon dropped below 10 ppm. Let us examine a case similar to our experimental sample (0.15 mm OD wire, 2 cm long) contaminated with 65 ppm carbon in which all of the carbon resided in the outer surface layers in the form of Fe_3C . Under such circumstances enough carbon is present for the first 10 or so atomic layers to be filled; thus, if the concentration fell below 10 ppm carbon only one monolayer of carbon compound could result which would probably be most inefficient in interrupting surfaces processes.

Further support for the proposition of carbide formation in the interface boundary is provided by the observed contact resistance (R_o) data. In Figure 13, a shift of one order of magnitude was required to correlate the theoretical curve (AFD) with the observed curve (afd), e.g. a move to A'F'D'. Curve AFD was derived under the assumption that ultra pure iron was the material in the interface, i.e. a resistivity of $9.7\mu\Omega\text{-cm}$. If instead the interface material was carbon rich iron, a shift in the bulk resistivity must be made to account for this change.

The best available data on the bulk resistivity of iron-carbon alloys (72) gives a value of $97\mu\Omega\text{-cm}$ (that required to correlate the above curves) at a carbon concentration of about 4 w/o, e.g. hypereutectoid iron-carbon alloys. Although the typical curves obtained resembled Figures 10 and 11, there were isolated instances where experimental observation indicated resistance values close to the low values expected for pure iron (insignificant

carbides present in interface), in these cases metallic adhesion characteristic of the bulk metal was observed. Since these results were not reproducible, a separate study is underway utilizing iron - 8 ppm carbon.

In summary let us describe the overall metallic adhesion process which we have considered thus far. There appears to be three areas of primary concern in such a description:

1. The pre-contact physical and chemical nature of the surface must be clearly defined.
2. Asperity deformation processes under load must be understood to provide an accurate description of the true contact area.
3. The unloading curve to the point of fracture must be clearly represented.

An examination of the overall mechanism will show how each of these facets are interrelated. For example, Figure 14 represents a hypothetical load (W) versus contact area (A) curve for two ideally elastic crossed rods, which is directly related to the observed R_0 versus W curves discussed previously. Three possible cases can be cited when the contact system is unloaded, depending on conditions existing in the interface. These are illustrated in Figure 14. The load cycle 0 to S is the same for all three cases.

Case I - No attractive forces along the interface. Fracture will proceed along curve S-0 to 0 at zero load. This has been observed with fully contaminated couples, i.e. under ambient conditions.

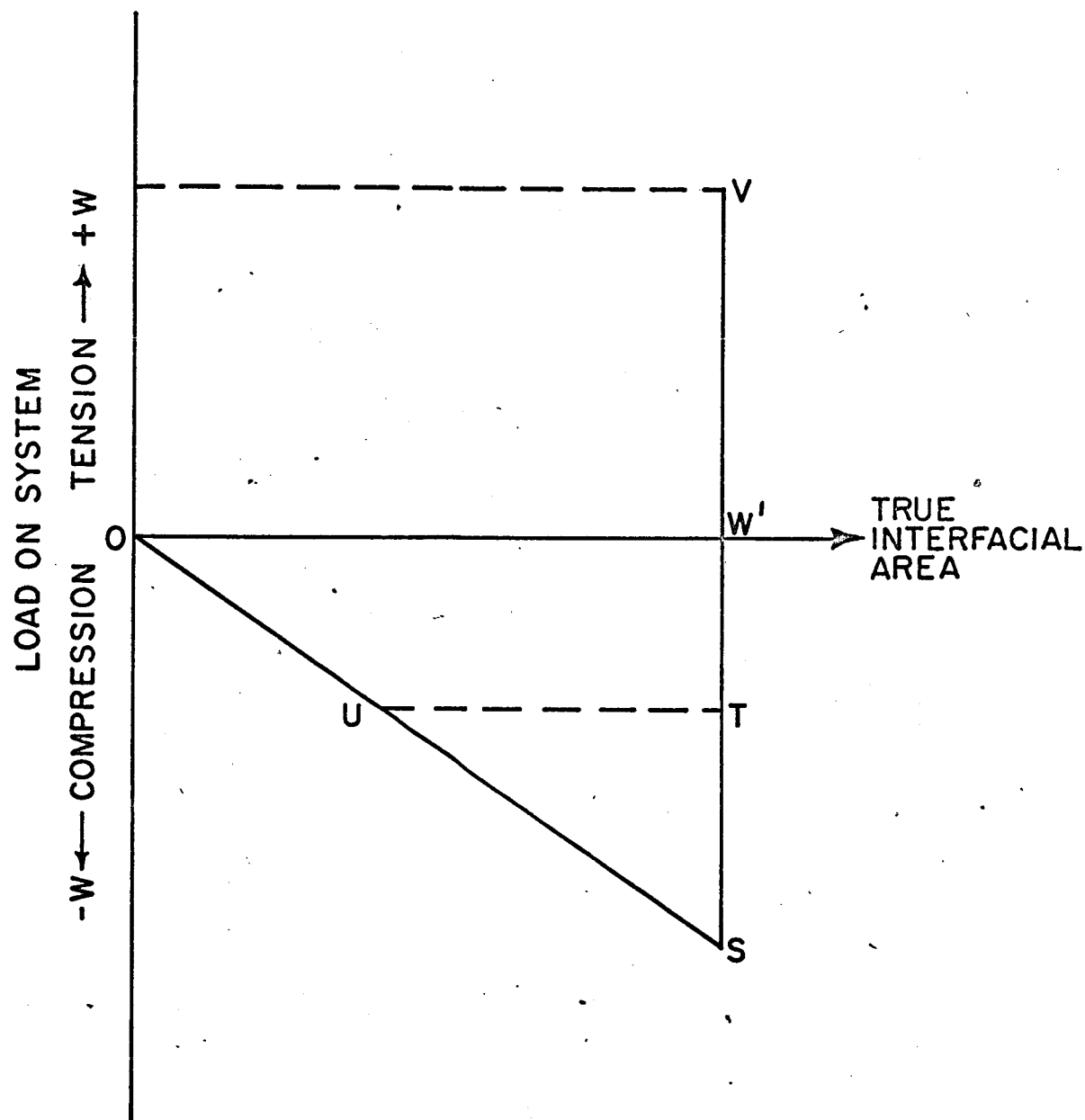
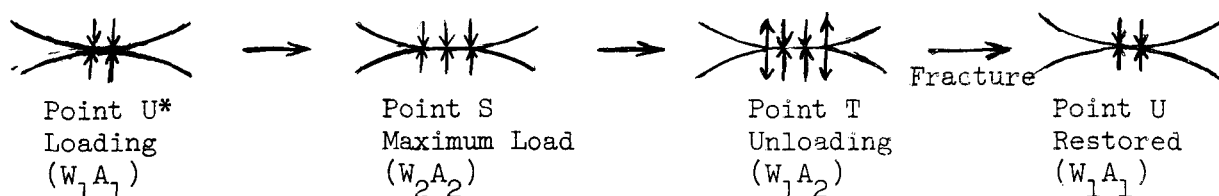


FIG. 14 LOADING CONDITIONS IN THE CONTACT INTERFACE

Case II - Interfacial attractive forces are equivalent to the strength of the bulk metal. Fracture will proceed along curve S-T-V as the load is reduced from compressive to the tensile mode. Fracture takes place at V. This type was also observed experimentally under conditions which approximate the ideal adhesion system as discussed in the introduction.

Case III - Weak attractive forces exist along the interface. The fracture curve will proceed along S-T-U-O. This curve is illustrated by Figure 9 of this study, in which iron and carbides are present in the interface.

Case I is probably an extreme of Case III, where a very weak interface constituent obscures the fracture steps actually present. The interesting point illustrated by Case III is that fracture can occur while the entire system is still under an applied compressive load. Bowden and Tabor (2) called this phenomena a "release of elastic stresses". As the load is reduced along S-T, the elastic system attempts to restore itself to its' original shape, e.g. at position U; however, due to the binding strength of the material in the interface, the restoration is retarded and the area held constant to position T. Balance is maintained, e.g. the central area of the interface is in compression (U) and outer edges under tension due to the elastic restoration force, until a crack is initiated in the outer-perimeter of the interface zone. At that point the system restores itself to point U by propagating a crack which causes the area (as seen from projection on O-W') to decrease from T to U.



*Points refer to Figure 14

If the load in an ideal adhesion system is reduced along S-T to $W=0$; the interface is under a tensile stress approximated by the area of the triangle OSW, which in turn suggests that the fracture point V is less than the true fracture stress of the bulk material by the amount of internal stress present at zero applied load.

The cycle U-S-T-U can be applied to a practical problem called "fretting," where a finite degree of fracture is observed even though the overall system is continuously under a compressive load during each cycle. It is obvious that clean material surfaces would be exposed when the fracture takes place along the interface during step UT.

A detailed mathematical analysis for a specific system of the fracture mechanics just outlined is beyond the scope of this investigation but shall be dealt with at a later time.

Creep

Although the prime purpose of this investigation did not intend to include the process of creep in the formation of an interface, preliminary studies were initiated. A significant amount of creep was observed in the loaded interface at room temperature, e.g. 0.17 Tmp. This process corresponds to what Tabor (61) has described as "junction growth" of two contacting surfaces subjected to a load for a period of time.

The creep process also lends credence to the proposed model of rough surface contact phenomena when two surfaces are brought together, i.e. plastic deformation of asperities as micro-deformation and elastic or plastic macro-deformation. Creep had not been considered previously for two bodies in elastic (macro) contact since it was thought that the plasticity of the material must be involved in the creep process. We can now consider the creep process of the asperities which were plastically deformed, even though the bulk elastic point had not been exceeded.

Figure 15 shows eight separate runs in which $\log R_o$ versus time is plotted. Again each datum point refers to a transfer point from the continuous "x-y" curve obtained from the run. The observed curves were displaced in transfer at the one second time coordinate such that all curves are superimposed at the point one second. The real deviation from 175 milliohms (1 sec) for all runs was ± 12 milliohms, and the reason for the shift is given below.

The runs were consecutive from 116 to 123; 116 was the first on the new contact point and 123 was the eighth on the same point. The flattening trend of the slopes suggests that a work hardening process has taken place. Several additional runs of this type of series gave generally the same type of curve.

A brief analysis of this process will illustrate the possibilities of a study of creep in a more detailed manner. Consider a relationship similar to that developed in equation 8, in which the area given by Holms relation (A_I) is related to the true area (A_N). If the true area is

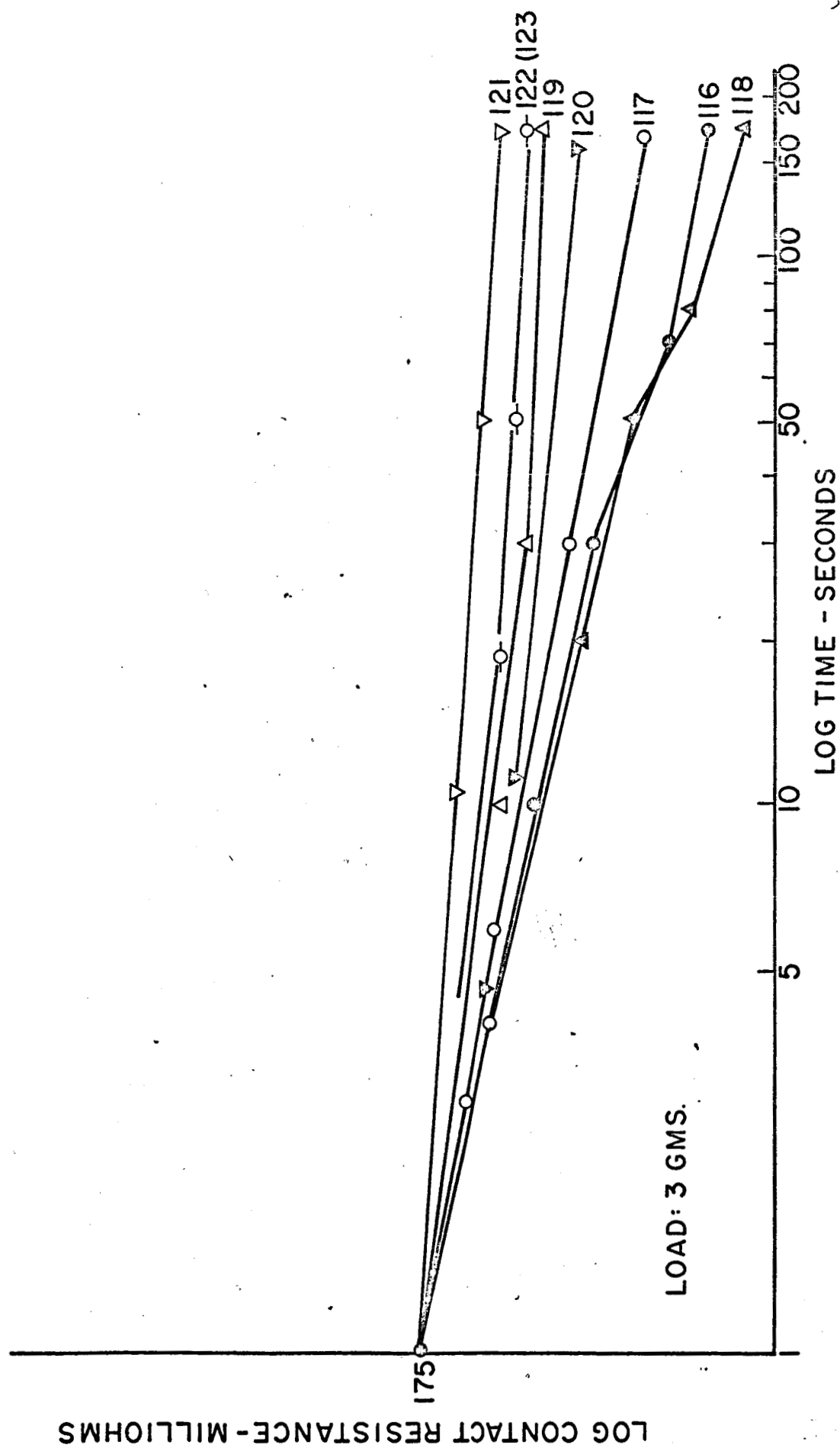


FIG.15 CONTACT RESISTANCE CREEP CURVES

studied as a function of time, Tabor (70) has shown that

$$A_N = \frac{W}{P} \quad \text{EQUATION 12}$$

where W is the load and P is the yield pressure in hardness studies.

Furthermore, P is related to time (t) by

$$P = A_1 t^{-1/m}$$

where

$$A_1 = A_5^{-1/m} \exp(-Q/RT)^{-1/m}$$

A_5 = system constant

Q = Activation energy of creep

R = Universal constant

T = Absolute temperature

m = Mechanical deformation constant

by substitution

$$A_N = \frac{W}{A_1 t^{-1/m}} \quad \text{EQUATION 13}$$

By proceeding as illustrated in the introduction, cf. equation 8, and making use of the time dependent equation we arrive at a relationship between R_c and t.

$$R_c = A_2 t^{-1/2m} \quad \text{EQUATION 14}$$

where

$$A_2 = \frac{\pi \rho^2 W A_1}{5.6 n^{1/4}} = \text{constant}$$

ρ = Bulk resistivity

n = Number of contact points

W = Load

By choosing the load in the creep experiment to exceed the load (1.3gm) where the number of contact points become constant, time becomes the only major variable in the expression. The slopes of the various creep curves shown in Figure 15 range from -0.2 for the new contact points and -0.05 for the multi contact portion of the curves. This suggests that the value of m must vary between 2.5 (for the ductile deformation process) and 10 (for the work hardening process). These values are consistent with values suggested by Tabor (70).

The creep investigations were not intended to be exhaustive; and therefore, the only valid conclusion that can be drawn from the data and correlations is that a technique has been developed which shows much promise for the study of interfacial deformation phenomena. The technique could possibly develop the mechanism of contaminant layer - real surface deformation processes, as well as the activation energy for creep in the surface layers.

IV. CONCLUSIONS AND RECOMMENDATIONS

1. Reproducible adhesion data has been provided by the development of an automatic continuous recording technique.
2. The slopes of the log-contact resistance (R_o) versus the log-load (W) curves were shown to closely relate to theoretical curves which consider surface asperity interactions as a continuous plastic process. Micro-elastic and microplastic asperity deformation phenomena are present in the contact interface although the bulk plastic yield strength of the material was not exceeded.

It is recommended that the absolute values of the observed resistance be further investigated to determine if their character is strictly metallic as assumed. This can be accomplished by studies employing cryogenic temperatures (Matthiessen's Rule) and alternating current. Microscopic and new instrumental methods are needed to give a clearer picture of the mathematic model of the asperities. Such studies will provide a more precise understanding of the contact area and inclusive material.

3. Gross metallic adhesion is not characteristic of the iron-65ppm carbon couple in the system investigated. Contamination of the sample surfaces by carbon, in the form of carbides from internal sources, appears to be a reasonable explanation for the barrier to adhesion in the system.

Investigations utilizing variations of the initial carbon content of the specimens (both lower and higher ppm carbon) are necessary to verify and expand the contamination model and adhesion characteristics proposed for the system. Gaseous removal and deposition of carbon or other contaminants

on the surface, accompanied by spectrographic analysis, will prove most useful in this case, as well as high energy electron diffraction studies. Also, by varying the temperature of the loaded couple and recording the fracture process, information can be provided as to the solubility of contaminants in the matrix along the interface plane. This would be very useful in lubrication studies.

4. Creep has been found to be a characteristic of the contact region, even under extremely light loading and ambient temperature conditions. The coefficients derived from contact resistance versus time plots indicate a plastic mechanism present in asperity phenomena which agrees with values from bulk plastic creep data.

A detailed analysis of the creep process should yield values for activation energies of creep in the interface region. Analysis of the effects of surface contaminants on creep would also produce much needed information.

BIBLIOGRAPHY

1. Eley, D.D., Adhesion, Oxford University Press, London (1961).
2. Bowden, F.P. and Tabor, D., Friction and Lubrication of Solids
Part I Oxford: Claredon Press (1950)
Part II Oxford: Claredon Press (1964).
3. Westwood, A.R.C. and Lye, R.G., "Surfaces and Interfaces in Materials Technology," presented at 14th Sagamore Conference: Surfaces and Interfaces - Physical and Mechanical Properties, New York (August 1967).
4. Bourgette, D.T., J. Metals, 12, 50 (1967).
5. Tabor, D., Grunberg, L., Robins, D., Metals and Materials 1, 9 (1967).
6. NASA Symposium, Interdisciplinary Approach to Friction and Wear, San Antonio, Texas (November 1967).
7. Bowden, F.P. and Tabor, D., Brit. J. Appl. Phys. 17, 1521 (1966).
8. Braithwaite, E.R., Solid Lubricants and Surfaces, MacMillian Company, New York (1964).
9. Tomlinson, A., Phil. Mag. 7, 905 (1929).
10. Hardy, W., Proc. Roy. Soc. A 112, 62 (1926).
11. Courtney-Pratt, J.S. and Eisner, E., Proc. Roy. Soc. A 238, 529 (1957).
12. Greenwood, J. A. and Williamson, J.B.P., Proc. Roy. Soc. A 295, 300 (1966).
13. Atkins, A. G. and Tabor, D., J. Inst. Metals 94, 107 (1966).
14. Goddard, J. and Wilman, H., Wear 5, 114 (1962).
15. Steijn, R.P., "Friction and Wear of Single Crystals," in Mechanisms of Solid Friction, Bryant, P.J., Lavik, M. and Solomon, G., eds, Elsevier Publishing Co., New York (1964).
16. Cocks, M., J. Appl. Phys. 33, 2152 (1962).
17. Eldredge, K. R. and Tabor, D., Proc. Roy. Soc. A 229, 181 (1955).
18. Keller, D.V., "On the Analysis of Metallic Adhesion Data," presented at ASTM-ASLE Conference on Adhesion, Toronto (May, 1967).

19. Johnson, K.E. and Keller, D.V., J. Appl. Phys, 38, 1896 (1967).
20. Johnson, K.E. and Keller, D.V., J. Vac. Sci. and Tech., 4, 115 (1967).
21. Gatos, H.C., "Structure of Surfaces and Their Interaction" presented at NASA Symposium (6) (November, 1967).
22. Keller, D.V., Ibid, discussion of "Friction and Adhesion," Merchant, M.E. (November, 1967).
23. Bond, G.C., Catalysis by Metals, Academic Press, New York (1962).
24. Haneman, D. and Grant, J.T.P., "Atomic Mating of Germanium Surfaces," paper C-7, 27th Physical Electronics Conference at Mass. Inst. Tech. (March, 1967).
25. Jona, F., "LEED Study of the Epitaxy of Si on Si," presented at 13th Sagamore Conference on Surfaces, New York (August 1966).
26. Conrad, H. and Rice, L., "Cold Welding of Copper in High Vacuum," presented at ASTM-ASLE Conference on Adhesion, Toronto (May, 1967).
27. Batzer, T.H. and Bunshah, R.F., J. Vac. Sci. and Tech., 4, 19 (1967).
28. Merchant, M.E., "Friction and Adhesion," presented at NASA Symposium (6) (November 1967).
29. Holm, R., Electric Contacts, Springer-Verlag Inc., New York (1967).
30. Gilbreath, W.P., "Definition and Evaluation of Parameters Which Influence the Adhesion of Metals," presented at ASTM-ASLE Conference on Adhesion, Toronto (May, 1967).
31. Roberts, R.W., "Clean Surfaces, Their Preparation and Characterization, Ibid, Toronto (May, 1967).
32. MacRae, A.V. "Techniques for Studying Clean Surfaces," presented at 13th Sagamore Conference on Surfaces, New York (August 1966).
33. Sikorski, M.E., Wear, 7, 144 (1964).
34. Sikorski, M.E., "The Adhesion of Metals and the Factors that Influence It," Bell Telephone Labs, Inc., Murry Hill, New Jersey (1963).
35. Milner, D.R. and Rowe, G.W., Met. Rev. 7, 433 (1962).
36. Semenov, A.P., Wear 4, 1, (1961).

37. Keller, D.V., "Status and Significance of Metallic Adhesion Research," presented at American Vacuum Society, New York (June, 1967).
38. Ham, J.L., Trans. ASLE, 6, 20 (1963).
39. Farnsworth, H.E., "Clean Surfaces" in The Surface Chemistry of Metals and Semi-Conductors, ed. Gatos, H.G., J. Wiley and Sons, New York (1960).
40. Pignocco, A.J. and Pellissier, G.E., J. Electro Chem. Soc., 112, 1188 (1965).
41. Farnsworth, H.E., J. Appl. Phys. 29, 1150 (1958).
42. Becker, J.A., Becker, E.J., Brandes, R.G., J. Appl. Phys. 32, 411 (1961).
43. Goodzeit, C.L. in Friction and Wear ed. Davies, R., Elsevier Publishing Co., Amsterdam (1959).
44. Keller, D.V., Wear, 6, 353 (1963).
45. Adamson, A.W., "Some Aspects of Surface Chemistry of Adhesion and of Friction," presented at ASTM-ASLE Conference on Adhesion, Toronto (May 1967).
46. Hordon, M.J., "Adhesion of Metals in High Vacuum," Ibid, Toronto (May 1967).
47. Butler, J.A.V., The Fundamentals of Chemical Thermodynamics, Part II, MacMillan Co., London (1934).
48. Erickson, J.C., in Advances in Chemical Physics, IV, Interscience Publishing Co., New York (1964).
49. deBruyn, P.L., "Some Aspects of Classical Thermodynamics," in Fundamental Phenomena in Material Sciences, ed. Bonis et al., Phenum Press, New York (1966).
50. Cahn, J.W. and Hilliard, J.E., J. Chem. Phys. 28, 258 (1958).
51. Buckley, D.H. and Johnson, R.L., "Marked Influence of Crystal Structure on Friction and Wear Characteristics of Cobalt and Cobalt-Base Alloys in Vacuum to 10^{-9} Torr," NASA TN D-2523 (1964).
52. Buckley, D.H. and Johnson, R.L., ASLE/Trans 8, 123 (1965).
53. Buckley, D.H. "Effect of Orientation on Friction Characteristics of Single-Crystal Berillium in Vacuum at 10^{-10} Torr," NASA TN D-3485 (1966).

54. Williamson, J.B.P., "Topography of Solid Surfaces," presented at NASA Symposium (6) (November 1967).
55. Archard, J.F., Nature, London 172, 918 (1951).
56. Saunders, W.M., Masters Thesis, Syracuse University (August 1967).
57. Greenwood, J.A., Brit. J. Appl. Phys., 17, 1621 (1966).
58. Went, J.J., Physica, 8, 233 (1941).
59. Kisluik, P., Bell System Tech. J., 37, 925 (1958).
60. Keller, D.V., Metallurgical Engineering Department, Syracuse University, Syracuse, New York, private communication.
61. Mulbearn, T.O. and Tabor, D., J. Inst. Metals, 89, 7 (1961).
62. Singer, J. and Anolick, E.S., J. Appl. Phys., 30, 195 (1959).
63. Jaoul, B. and Gonzales, D., J. Mech. Phys. Solids, 9, 16 (1961).
64. Hume-Rothery, W., The Structures of Alloys of Iron Pergamon Press, New York (1966).
65. Christian, J.W., The Theory of Transformations in Metals and Alloys, New York (1965).
66. Bibly, M.J., Parr, J.G., J. Iron Steel Inst., 202, 100 (1964).
67. Sewell, P. and Mitchell, D., Chemistry Department, Nat. Research Council, Ottawa, Canada, private communication.
68. Kaplan, D. and Hussey, R. Ibid, private communication (also see Linstrand, E., Acta Met. 3, 431 (1955)).
69. Pignocco, A. and Pellisier, G., U.S. Steel Research, Monroeville, Pennsylvania, private communication. Also mentioned in J. Electro chem Soc., 112, 1188 (1965).
70. Tabor, D., Atkins, A.G. and Silvero, A., J. Inst. Metals 94, 369 (1966).
71. Lawson, A.W., "Effects of Hydrostatic Pressure on the Electrical Resistivity of Metals," Progress in Metal Physics, 6 ed. B. Chalmers, Pergamon Press, New York (1956).
72. ASM Metals Handbook, VI, 8th Edition, (1961).

BIOGRAPHICAL DATA

Name: Thomas Martin McNicholas

Date and Place of Birth: May 3, 1939; Brooklyn, New York

High School: Saint Michaels (D.H.S.), Brooklyn, New York

College: Polytechnic Institute of Brooklyn
Brooklyn, New York
B.S. (Metallurgy), 1961

Graduate Work: Syracuse University, Syracuse, New York
Research Assistant 1966-1968

University of California
Los Angeles, California

Experience: Graduate Research Assistant
Syracuse University Research Institute
Syracuse, New York

Materials and Process Engineer
Lockheed Aircraft
Burbank, California

Plant Metallurgist
Harvey Aluminum
Torrance, California